

Article

# The Effects of Chloride on the High Temperature Pressure Oxidation of Chalcopyrite: Some Insights from Batch Tests—Part 2: Leach Residue Mineralogy

Robbie G. McDonald 

CSIRO Mineral Resources, Australian Minerals Research Centre, 7 Conlon Street, Waterford, WA 6152, Australia; robbie.mcdonald@csiro.au

**Abstract:** The complete reaction of chalcopyrite at  $\geq 220$  °C under pressure oxidation conditions (10 or 20% *w/w* pulp density,  $PO_2$  700 kPa) is a clean process producing a residue consisting of hematite and un-reacted gangue minerals. However, when the process water contains chloride ions, covellite intermediate formation is significant and subsequently generates elemental sulphur that can persist for up to 60 min. Increasing the temperature to 230 °C reduces this time, although the dissolution of copper and the oxidation of sulphur still follows non-parallel reaction pathways. At 245 °C, the production of elemental sulphur in the presence of moderate chloride levels, 15 g/L, is no longer significant. The effects of other chemical additions (including enhancement of aluminium content) are also examined. Particular emphasis is given to the mineralogy of the leach residues and the department of iron in these residues to various phases that include hematite, basic ferric sulphate and natrojarosite. The residues are found to also contain a number of other intermediate phases in addition to covellite and sulphur, such as antlerite and clinoatacamite, depending upon the leach conditions employed.

**Keywords:** chalcopyrite; chloride; pressure oxidation; covellite; clinoatacamite



**Citation:** McDonald, R.G. The Effects of Chloride on the High Temperature Pressure Oxidation of Chalcopyrite: Some Insights from Batch Tests—Part 2: Leach Residue Mineralogy. *Minerals* **2023**, *13*, 1162. <https://doi.org/10.3390/min13091162>

Academic Editor: Jean-François Blais

Received: 28 June 2023

Revised: 26 August 2023

Accepted: 28 August 2023

Published: 31 August 2023



**Copyright:** © 2023 by the author. Licensee MDPI, Basel, Switzerland. This article is an open access article distributed under the terms and conditions of the Creative Commons Attribution (CC BY) license (<https://creativecommons.org/licenses/by/4.0/>).

## 1. Introduction

In part 1 of this study [1], the solution chemistries associated with high-temperature pressure oxidation of chalcopyrite in process water of various compositions under batch conditions were described and compared. More specifically, the effects of chloride ions in the process water upon the system were considered. This second part of the study focuses on the mineralogical changes that accompany the experiments described in part 1.

It is widely acknowledged that high-temperature pressure oxidation of chalcopyrite concentrates (using good quality process water) produces residues that contain hematite and/or basic ferric sulphate in addition to poorly leached and/or inert gangue minerals originally present in the concentrates (e.g., [2]). In comparison, iron reports to hematite under oxidative ammoniacal conditions, such as those employed in the Arbitrator process [3]. The nature of leach residues generated during the alkaline glycine leaching of chalcopyrite appears to be more complicated owing to the low extent of leaching found under the conditions studied, facilitating the formation of both neutral and basic copper-containing compounds [4]. A more recent study that examined the impact of mechanical activation upon the alkaline glycine leaching of chalcopyrite resulted in significantly greater copper extractions and produced leach residues that contained copper glycinate ( $Cu(NH_2CH_2COO)_2$ ) which could be recovered, covellite, maghemite ( $\gamma-Fe_2O_3$ ) and quartz [5].

While rare, deviations from the expected mineralogy of high-temperature pressure oxidation leach residues formed from chalcopyrite have been described [6,7], as have variations for residues generated using low-to-medium pressure oxidation regimes [8]. Subsequently, several detailed studies of residues generated by the CESL process have been conducted [9–11]. The study of Sahu and Asselin [9] identified goethite ( $\alpha-FeOOH$ )

in a number of residues produced under CESL conditions and in one instance, ferrihydrite ( $\delta$ -FeOOH). The use of a two-stage sequential extraction method confirmed the presence of amorphous/poorly crystalline iron oxides (e.g., ferrihydrite) and gave estimates of the amounts. In a follow-up study, the application of QXRD analysis to CESL process residues indicated poor correlation with the elemental analysis for iron, assuming all materials were crystalline [10]. The addition of an alumina internal standard enabled the amounts of amorphous/poorly crystalline iron oxide phases, suspected to be ferrihydrite or a mixture of iron oxides/hydroxides, to be determined. This was confirmed by selective extraction of these phases using hydroxylamine hydrochloride. Further to this, Mössbauer spectroscopy indicated poorly crystalline hematite in the samples, though it is not clear whether this material was selectively extracted. It has been reported that nano-sized hematite does not generate the standard XRD pattern associated with material for which the crystals have larger coherently diffracting domains [12].

The study of Javed et al. [11] examined the residues formed in the presence of copper in the sulphate–chloride systems at 150 °C where chloride was added as  $\text{CuCl}_2$  and  $\text{FeCl}_3$ . Although goethite was noted to form when the final acid concentration was low (12.5 g/L) the dominant phase formed was normally hematite. Copper losses to the residue decreased with increasing acidity and when hematite seed was added, while the extent of iron precipitation increased with increasing retention time, and increasing copper and chloride concentrations, both up to 30 g/L.

The formation of intermediate copper-containing phases during oxidative leaching of chalcopyrite has long been recognised, e.g., [13]. The work of Chaiko et al. [14] concluded that the formation of only a small amount of a covellite-like phase, best formulated as  $\text{Cu}_6\text{S}_6$ , facilitates the low-temperature leaching of chalcopyrite in the FLSmidth® Rapid Oxidative Leach (ROL) process. In contrast with the non-oxidative processing of chalcopyrite, X-ray analysis did not detect the formation of other secondary sulphides such as digenite ( $\text{Cu}_{1.8}\text{S}$ ) and chalcocite ( $\text{Cu}_2\text{S}$ ). For the ROL process, the formation of covellite at significant levels was concluded to be parasitic with respect to dissolution. Hence control of the Eh and pH were employed to limit covellite formation as the mechanism for accelerating chalcopyrite leaching.

Even at high temperatures (180–200 °C), the formation of copper sulphide intermediates has been noted, e.g., [15]. An upgrade in the copper content of chalcopyrite has been described under oxidising conditions by Bartlett [16] and Muszer et al. [17] who generated predominantly digenite and covellite, respectively. In comparison, the study of Hawker et al. [18], which appears to have been conducted at Eh controlled by the addition of ferric sulphate, preferably formed covellite.

Although the topic has a rich history, e.g., [19–22], there has been a significant renewed focus upon the non-oxidative/metathetic upgrade/purification of chalcopyrite concentrates and several studies describe the mineralogical transformations that occur, e.g., [23,24]. This approach has been targeted for practical application: Fomenko et al. [25] describe an approach referred to as hydrothermal alteration that enables the upgrade of chalcopyrite concentrate and partial removal and recovery of co-present base metals, namely zinc and lead, whereas the reaction of sphalerite with copper-containing solutions can also form digenite and chalcocite [26]. This involves a step to generate copper-containing solution that is employed in the hydrothermal alteration step (which can be conducted without and with partial oxidation) and enables the rejection of other elements. This approach is the same in principle as that of Dunn [27], whereby a non-oxidising step that uses an acidic copper sulphate solution generated by oxidative treatment of a copper sulphide source is employed to upgrade the copper content of the final product. A similar application was described in the study of Kritskii et al. [24]. In comparison, the application of copper metathesis reactions in the commercial processing of nickel matte is well known, e.g., Van Wyk et al. [28], and has also been suggested for the enrichment of copper concentrate via the removal of copper from leach liquor derived from mixed nickel-copper concentrates [29].

It has previously been noted that elemental sulphur can form and persist at high temperatures (220 °C) when sodium chloride is added to the system [6]. Other studies have similarly noted the presence of small amounts of sulphur in leach residues produced from pyrite at high temperatures in the presence of chloride, e.g., [30]. In the piloting of the Platsol process, which employed a lixiviant containing 10 g/L chloride, the total leaching time was 66 min although most of the metals were extracted within around 20 min [31]. The additional time combined with recycle of the leached residue was shown to ensure complete oxidation of the elemental sulphur (in addition to marginally improving metal extractions); it is noted here that the potential for sulphur intermediate formation in this process was inferred [32], but was not specifically confirmed. In comparison with other studies undertaken in the presence of chloride, King et al. [33,34] found that elemental sulphur is present in residues from the pressure oxidation of copper concentrates (150 g in 1 L lixiviant) at temperatures of 180–190 °C after 3 h but at temperatures of 200–220 °C there was virtually no elemental sulphur.

Finally, it has been shown that basic copper salts can form during chalcopyrite leaching, depending upon the starting conditions [8]; this means post-leach pH adjustment may be required for more efficient copper recovery. This approach is employed in the CESL process [35] and may be advantageous for copper removal (as  $\text{Cu}_2(\text{OH})_3\text{Cl}$ ) after sodium chloride-based oxidative leaching of nickel sulphide ore/concentrates [36]. Conversely, pH control to below 2.5 is used to prevent atacamite formation in the HydroCopper<sup>®</sup> process where the concentration of NaCl is targeted to 280 g/L [37]. It has been noted that antlerite,  $\text{Cu}_3(\text{SO}_4)(\text{OH})_4$ , is formed in treating CESL process leach liquor [38] and this is presumably determined by a high sulphate-to-chloride ratio in the liquor. In comparison, copper precipitation from NaCl solutions at 80 °C and a high pH of 9.5 also results in the formation of cuprite,  $\text{Cu}_2\text{O}$ , and tenorite,  $\text{CuO}$ , in addition to atacamite and clinoatacamite [39]. At lower temperatures, 30 °C, atacamite is formed from NaCl and  $\text{NH}_4\text{Cl}$  solutions during chalcopyrite leaching [40].

Following McDonald [1], the present study was conducted to examine the (batch processing) effects of various chloride-containing process fluids upon the mineralogical transformations of chalcopyrite concentrate to residue components. Comparisons are made to systems without added chloride and those for which other additives have been employed. The changes occurring as a function of time are discussed with respect to the corresponding process fluid compositions. The study represents the first comprehensive comparison of the impact of high temperature, and pressure oxidation conditions on the mineralogical changes that can occur during the batching processing of a chalcopyrite concentrate.

## 2. Experimental

The details of the experimental method, experimental conditions and analytical methods have previously been described in part 1.

Solid sub-samples were weighed with the addition of 10% fluorite (internal standard) and lightly milled in absolute ethanol using a McCrone micronizing mill (McCrone, Westmont, IL, USA) and dried in air. XRD traces of the ground, dried samples were mostly obtained using a Philips Xpert diffractometer (Philips, Almelo, The Netherlands) operated at 40 kV and 40 mA, and the following acquisition conditions:  $\text{Co K}\alpha$  radiation, 5–120°  $2\theta$ , 0.05°  $2\theta/\text{step}$ , 1.5°  $2\theta/\text{min}$ , primary and secondary Soller slits installed (receiving slit 0.2 mm).

The XRD patterns shown in Section 4.5.8 were obtained using a PANalytical high-resolution multi-purpose powder diffractometer (Empyrean) (Malvern Panalytical, Malvern, UK) operated at 40 kV and 40 mA. The instrument optics consisted of a Bragg–Brentano high-definition monochromator, with fixed divergence, 0.5°, and anti-scatter, 1°, slits, placed in the incident X-ray beam, a programmable anti-scatter receiving slit, and incident and receiving 0.02 rad soller slits inserted. A PIXcel3D photon counting X-ray detector was

used to collect the data over an angular range of 5–130° 2 $\theta$  with a continuous scan mode for 2 h.

Rietveld refinements were conducted using Brüker-AXS TOPAS software (versions 3 and 4.2, Bruker, Billerica, MA, USA) and a verified set of crystal structure models that can be found within the FIZ Karlsruhe 2011 ICSD [41] or the ICDD PDF-4+ 2022 databases [42]. Most models employed were taken from published crystal structures except for basic ferric sulphate, Fe(OH)SO<sub>4</sub>, for which a calibrated Pawley fit was obtained to generate a suitable phase quantification model. Modelling of this phase using atomic coordinates requires the order-disorder character, viz., the simulation of stacking sequences as described by Ventruti et al. [43], to be included; the Pawley fit was confirmed by analysis of samples containing known amounts of basic ferric sulphate to give acceptable quantification of this phase.

### 3. Ore Characterisation

Quantitative X-ray Diffraction (QXRD) analysis of the concentrate employed in the present study indicates that the material consists of 71% chalcopyrite (CuFeS<sub>2</sub>), 11% quartz (SiO<sub>2</sub>), 7% pyrite (FeS<sub>2</sub>), 8% talc (Mg<sub>3</sub>(Si<sub>2</sub>O<sub>5</sub>)(OH)<sub>4</sub>), 1.5% clinocllore (e.g., (Mg,Fe)<sub>5</sub>Al(Si<sub>3</sub>Al)O<sub>10</sub>(OH)<sub>8</sub>) and a trace amount of elemental sulphur. The calculated elemental content based upon QXRD was in excellent agreement with chemical analysis obtained using a Varian Vista Pro ICP-OES (Varian, Palo Alto, CA, USA) and LabFit carbon and sulphur analyser (LabFit Pty Ltd., Perth, WA, Australia) instruments. These data are given in Table 1.

**Table 1.** Analytical data for the chalcopyrite concentrate.

Elemental Content (% w/w)							
Cu	Fe	Al	Mg	Ca	Si	Na	S
24.5	26.9	0.240	1.14	0.015	4.35	0.008	31.4

## 4. Results

### 4.1. Summary of Dissolution Behaviour

The first paper in this series, Part 1 [1], described insights provided by the dissolution of various elements from the chalcopyrite concentrate with a specific focus on the behaviour of copper, iron and sulphur. A summary of the results in terms of the concentration ranges of dissolved elements and the ranges of extraction at the conclusion of the experiments is provided in Table 2; these data were segregated based on the chalcopyrite pulp density (% w/w) used.

**Table 2.** Analytical data for the chalcopyrite concentrate \*.

Pulp Density (% w/w)	Cu	Fe	Al	Mg	Ca	Si	Na	S
Elemental concentration range (g/L)								
10	24.4	0.54	0.25	0.55	0.23	0.51	0.01	31.5
	29.5	1.49	0.57	3.23	0.25	0.54	10.3	34.0
20	58.3	0.21	0.21	1.18	0.03	0.04	0.03	60.1
	68.5	21.0	1.35	3.72	0.52	0.51	64.9	89.6
Extraction range (%)								
10	98.9	1.8	68.8	50.6	97.9	9.3	-	96.5
	99.3	4.9	87.3	87.9	99.5	9.8	-	97.9
20	97.2	3.5	10.0	38.3	82.6	0.4	-	66.2
	99.8	24.8	80.0	80.7	99.4	4.2	-	98.1

\* Upper and lower values in each entry represent minimum and maximum values, respectively.

The data indicate that high copper and corresponding sulphur tenors and extractions were obtained. Iron concentrations and extractions were typically low due to iron hydrolysis forming hematite; however, when additional up-front acid was added and/or a chloride addition (as NaCl) of 100 g/L was employed the iron concentration was higher; the maximum value of 21.0 g/L corresponded to acid and chloride additions of 100 g/L. In contrast to copper, the extraction data for sulphur spanned a broader range when the pulp density was 20% *w/w*. This was due to losses as basic iron sulphate phases and where formed, natroalunite, as discussed in later sections; for clarity, note here that basic iron sulphate phases refers to both basic iron sulphate, Fe(OH)SO<sub>4</sub>, and natrojarosite, NaFe<sub>3</sub>(SO<sub>4</sub>)<sub>2</sub>(OH)<sub>6</sub>.

The concentrations of other elements, except for Na which varied due to sodium salt (mostly NaCl) addition, were much smaller than for copper and sulphur. Variations in both these values and the corresponding extractions were attributed to concentrate sub-sample variation of the contained mineralogy.

#### 4.2. Overview of Residue Mineralogy

A range of non-chloride- and chloride-based systems was employed in this study to assess the pressure oxidation behaviour of a single chalcopyrite concentrate as described by the experimental conditions given in Part 1 [1]. A number of residue phases were generated and the maximum contents for each of these across all the residues produced, including those taken during experiments, is presented in Table 3; note these values are normalised relative to the amount of concentrate used whereas data presented in subsequent sections are compositions in the residue samples. The following sections provide more detail of the conditions that give rise to the formation of these various phases.

**Table 3.** Summary of residue phases formed and their contents normalised to the chalcopyrite concentrate addition.

Phase	Max. (% <i>w/w</i> )	Phase	Range (% <i>w/w</i> ) *
Hematite	70.5	Antlerite	1.5–9.3
Alunite/jarosite #	60.0	Clinoatacamite	6.1–16.1
Basic ferric sulphate	59.4		
Covellite	36.9		
Sulphur	20.2		

# Alunite/jarosite phases generally dominated by natrojarosite having a low aluminium content unless otherwise indicated in sections below; \* Range of contents given when these phases detected.

#### 4.3. Copper Metathesis

Experiments to understand the reactions involved in secondary copper sulphide enrichment and iron sulphide enrichment via metathetic reactions with cupric sulphate at temperatures up to 200 °C were first conducted more than a century ago [44]. At about the same time, two other studies examined the enrichment of copper ores in the presence of hydrogen sulphide [45] and in the copresence of hydrogen sulphide and a source of iron, such as ferrous sulphate, ferrous sulphide or magnetite [46].

Detailed studies of the metathesis process occurring when chalcopyrite is heated with cupric sulphate in the absence of oxygen have been published and ascribed to the following reactions [22,23]:



This gives an overall reaction:



The corresponding reaction in a chloride-based system is:



The metathetic conversion of chalcopyrite to form digenite in the presence of oxygen has also been studied, e.g., [16,21]. This apparently occurs when oxygen transfer to the mineral slurry is not fast enough to maintain a sufficiently high oxidation potential for copper dissolution; Bartlett [16] was able to demonstrate high conversion of chalcopyrite to digenite on a continuous basis at 200 °C by controlling the stoichiometric ratio of oxygen to chalcopyrite feed into an autoclave and thereby maintain the system Eh at around 500 mV SHE. Conversely, the complete leaching of chalcopyrite particles (150 µm) in a matter of minutes has been reported by Viramontes Gamboa et al. [47] who employed a microelectrode to apply a potential in the transpassive region (1.44 V SHE), whereby around 90% of the sulphide was oxidised to elemental sulphur.

Metathesis studies reported by Hawker et al. [18] employed a chalcopyrite concentrate and investigated a range of experimental parameters: 120–200 °C,  $[\text{Cl}^-]$  30–120 g/L, initial mass ratio Cu(solution):Fe(solids) 0.5–2:1 (normally 1.33:1) and reaction time 0.5–4 h. The optimum conditions for the conversion of chalcopyrite (and bornite), i.e., with respect to copper precipitated and iron leached, to mainly form covellite and lesser digenite were indicated to be: 180–200 °C,  $[\text{Cl}^-]$  75 g/L, initial mass ratio Cu(solution):Fe(solids) 0.5–1:1 and reaction time 1 h. When more digenite was formed, the amount of basic copper chloride decreased, and this is consistent with Equation (4) whereby increased acid formation is expected to either result in dissolution or hinder the formation, of the basic copper salt(s); it is also consistent with the data presented by Byrne et al. [48] which indicated the basic copper salt formed to be atacamite.

The study of Kritskii et al. [24] with chalcopyrite concentrate, but in the presence of copper sulphate, also investigated a range of experimental parameters: 150–230 °C, initial mass ratio Cu(solution):Fe(solids) 1.2–3.3:1, acid concentration 20–120 g/L; optimum parameters were estimated to be a temperature of 230 °C, initial mass ratio Cu(solution):Fe(solids) 1.8–1.9:1, acid concentration 20–40 g/L, and reaction time 60–100 min as this allows a concentrate with 51%–52% Cu and residual copper concentrations as low as 0.08–0.13 g/L to be obtained. The leach residue contained a mixture of copper sulphides mainly consisting of digenite,  $\text{Cu}_{1.8}\text{S}$ , and djurleite,  $\text{Cu}_{1.94}\text{S}$ .

The fundamentals of non-oxidative upgrading of chalcopyrite have been investigated using in-situ XRD and XAS by Chaudhari et al. [49]. They found metathesis to form covellite and digenite involves pseudomorphic mineral replacement reactions that occur by a coupled interface dissolution and reprecipitation mechanism [50]. Based upon XANES, rapid reduction of aqueous cupric to cuprous ions was indicated while iron reported to solution in the ferrous state, and from which szmolnokite,  $\text{FeSO}_4 \cdot \text{H}_2\text{O}$ , was shown to precipitate. Although Cu(I) is dominant over Cu(II) at high temperatures the presence of both Cu(I) and Cu(II) are favourable for the formation of covellite. Based upon the study of Harmer et al. [51] it has been proposed that Fe(III) can catalyse the oxidation of  $\text{S}^{2-}$  to form  $\text{S}_2^{2-}$ , also important for the formation of metathesis products. Such a reaction appears to be critical to the co-existence of Fe(II) and significant Cu(I) in solution derived from the non-oxidative treatment of chalcopyrite; it is also consistent with Cu(II) catalysis of disulphide ion formation.

In the current study, when 15 g/L chloride was added as cupric chloride with no up-front acid addition, the net extraction of copper was faster during the first 5 min [1], notwithstanding that the copper present in the (covellite) metathesis product formed by the reaction of cupric ion with chalcopyrite during heat-up had also leached during this period (see Figure 1). The initial copper addition prior to heat-up, 13.8 g/L, represented 23.7% of that in the copper concentrate. As there was a small amount of residual dissolved copper present when oxygen was introduced into the system, 2.9 g/L, this enhanced leaching rate is consistent with the role of the copper(I)/copper(II) oxidation-reduction couple in facilitating the reaction [52]. Notably, however, the ratio of dissolved copper to that in the

solids is well below that employed for the non-oxidative upgrading of copper concentrates. Based on the information provided by Dunn [27], this ratio is somewhere between 150% and 220% while Peterson and Wadsworth [22] and Hawker et al. [18] employed ratios of 200% and 148%, respectively, in their fundamental studies. In the present study, the extent of covellite formation was relatively small, comprising 14% of the solids present at the end of the heat-up period [1]. No digenite was detected and this is also consistent with the low acid concentration which was ~0.1 g/L. This may also indicate that most of the reaction had taken place at lower temperatures and prior to reaching the target temperature (220 °C) given higher temperature is more favourable for the stability of Cu(I) ions, and therefore, digenite formation, as found by Chaudhari et al. [50].

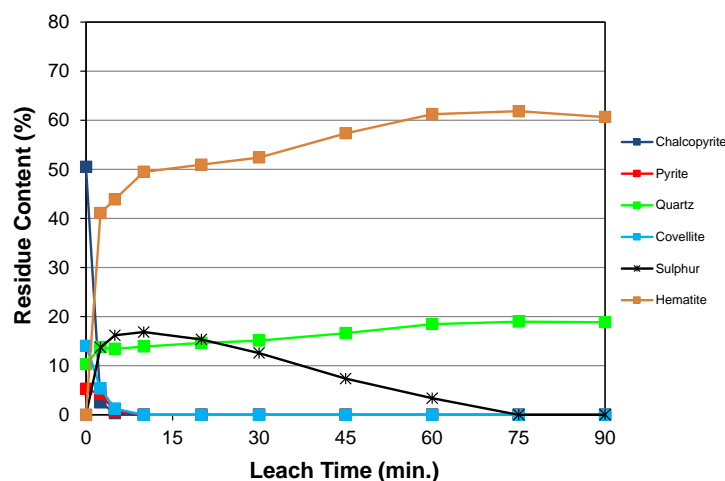


**Figure 1.** Mineralogy of the leach residue obtained during the leaching of chalcopyrite concentrate ( $P_{100} - 45 \mu\text{m}$ ) under pressure oxidation conditions (220 °C, 700 kPa  $\text{O}_2$ , 20%  $w/w$  pulp density, 15 g/L chloride). Chloride added as cupric chloride ( $\text{CuCl}_2 \cdot 2\text{H}_2\text{O}$ ).

Aside from covellite formation during the heat-up period, the data in Figure 1 indicate rapid leaching of chalcopyrite and covellite, and simultaneous formation of elemental sulphur and hematite once pressure oxidation commenced. The sulphur generated slowly oxidises throughout the experiment even though around 96% of the copper had leached and the free acidity was 6.3 g/L [1], and the chalcopyrite content of the leach residue had decreased to 0.4%, all after 5 min. At this time around 95% of the sulphur in the residue is in elemental form and the ratio of oxygen usage to copper extraction is expected to be near optimum. This also clearly demonstrates the decoupling of the iron and sulphur oxidation pathways, with the former being significantly quicker. Although further work is required to confirm, it is hypothesised that a significant fraction of the copper remaining in the residue was associated with hematite that formed rapidly given also that no pyrite (a potential sink for dissolved copper) was detected after 5 min. As the sulphur was oxidised and free acidity increased, some of the hematite dissolved releasing associated copper while dissolution-precipitation of the hematite phase will have occurred more rapidly with increasing free acidity as the system approached equilibrium. The final copper content of the residue, 0.56%, is not dissimilar to the zinc content found in hematite generated in the zinc industry, 0.5%–1% [53].

The iron content of the liquor after heating up being 16.4 g/L confirms its presence in the ferrous form, as the solubility of ferric iron (relative to hematite formation) is significantly lower [54]; the data of Liu et al. [55] indicate that the solubility of hematite in 10 g/L sulphuric acid will generate a Fe(III) concentration of 0.47 g/L at 230 °C, a value expected to lower significantly as the acid concentration drops below 1 g/L. The phase szomolnokite,  $\text{FeSO}_4 \cdot \text{H}_2\text{O}$ , which has a decreasing solubility in water with increasing temperature, e.g., [56], is expected to be present but to dissolve (during cooling) when samples are taken from the autoclave. Furthermore, the solubility of this phase at 200 °C

increases in the presence of sulphuric acid [57]. The study of Chaudhari et al. [49] found when reaction (1) is dominant relative to reaction (2) that szomolnokite is formed (although there was a low initial concentration of acid present in the system) and that upon cooling, this phase dissolves. In the present study, the findings are consistent with the metathesis reaction:



Cai et al. [58] proposed that covellite forms in hydrochloric acid at temperatures below 100 °C via simultaneous dissolution and re-precipitation resulting in pseudomorphic replacement of the chalcopyrite. A similar conclusion as noted previously was reached by Chaudhari et al. [49] while such a mechanism has also been proposed for the replacement of pentlandite by violarite [59]. As part of the reaction mechanism involved here, it is expected that dissolved Cu(I) would be rapidly oxidised by Fe(III), e.g., [60,61]. This is also consistent with the conclusion of Pearce et al. [62] and the recent study of Li et al. [63] that the oxidation states of copper and iron in chalcopyrite are +1 and +3, respectively; a survey of this and other related studies by Conejeros et al. [64] suggests there is still controversy on this point.

That an equilibrium between cupric and cuprous ions exists was also demonstrated for the cupric chloride leaching of chalcopyrite [65]. Once this equilibrium was established, any regeneration of cupric ion occurs via the reduction of elemental sulphur to form CuS, which was proposed to explain why cupric chloride leaching of chalcopyrite may not proceed to completion if cupric ion addition is insufficient in the absence of a secondary oxidant. In comparison, the formation of secondary covellite was demonstrated under HydroCopper® process conditions at  $\text{pH} \leq 1.4$  by Lundström et al. [66] in the absence of oxygen purging. Based on the experimental details provided, the molar ratio of Cu(II) to chalcopyrite was at least 6.56 compared to values of at least 4.74 for the study of Chaudhari et al. [49] and 3.68 for that of Cai et al. [58]; in all instances these ratios were well above the stoichiometric requirement for reaction (5), and as indicated earlier, well above the value of 0.237 used here.

It is recognised that the electronic structure of covellite is not consistent with copper being in the +2 state [67–69], a point noted when the crystal structure of this mineral was first published [70]; the unit cell was proposed to contain one  $\text{Cu}^{2+}$  and  $\text{S}^{2-}$ , and two  $\text{Cu}^+$  with two  $\text{S}^-$  (as the  $\text{S}_2^{2-}$  ion) species. Thus, it appears the formation of covellite involves stabilisation of the +1 state, initially in solution by the formation of cuprous chloride complexes and, in the solid state via the formation of the  $\text{S}_2^{2-}$  ion. That cuprous ions must be present for covellite to form is also consistent with a range of published synthesis methods that use, for example, cupric salts in combination with a reducing agent such as thiourea [71,72] or sodium thiosulphate [73,74]; given, however, that “covellite-like” nanoparticles can be synthesised from copper sulphate and sodium sulphide [75] is consistent with  $\text{Cu}^{2+}$  oxidation of  $\text{S}^{2-}$  to form  $\text{S}_2^{2-}$  ions. The presence of cupric ions in the covellite structure is indicated by X-ray photoelectron spectroscopy measurements, e.g., [76] and references therein. It is, however, interesting to note Almeida et al. [77] detected covellite formation by Raman spectrometry during anodic polarisation of chalcopyrite electrodes in nitric acid though it is expected Cu(I) will not be stable in solution. This suggests a mechanism that may not involve dissolution-reprecipitation steps.

#### 4.4. Reaction of Chalcopyrite with Acid

Rather than metathesis, which is concluded to occur via the solid-state exchange of cupric for ferrous ions, e.g., [14], covellite formation has also been noted to occur in hydrochloric and nitric acids at the surface of “polished” chalcopyrite (see also [77]). Similarly, it was found that heating chalcopyrite with added sulphuric acid, here either 30 g/L or 100 g/L, prior to commencing pressure oxidation resulted in the formation of a small amount of covellite, ca. 3%–4%, along with the dissolution of substantial iron relative

to copper [1]). It has been proposed that H<sub>2</sub>S formation should occur according to the following reaction:



However, no smell of this gas was noticed when samples were taken prior to oxygen injection; Ghahremaninezhad et al. [78] have also indicated they are not aware of H<sub>2</sub>S formation during the acid-based leaching of chalcopyrite and although this was reported to occur for acidic chloride solution in the subsequent study of Recalde Chiluiza and Navarro Donoso [79], they indicated that quantitative determination of the amount of H<sub>2</sub>S formed could not be undertaken. For comparison, the sulphation of chalcopyrite via reaction with 75%–96% sulphuric acid at 180–260 °C generated trace amounts of H<sub>2</sub>S [80].

#### 4.5. Impacts of Chloride and Other Additives

##### 4.5.1. Effects of Pulp Density and Added Chloride

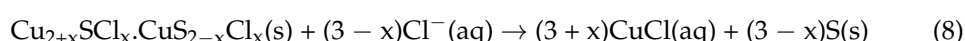
At low pulp density (10% *w/w*), the reaction of chalcopyrite was rapid and essentially complete within 10 min both without and with 15 g/L added chloride (Figure 2A,B). During the first few minutes of the reaction, covellite formed as an intermediate product. A similar finding was made at a higher pulp density of 20% *w/w*, and a covellite content of ~28% was noted in the 2.5 min sample when 15 g/L chloride was present but just 9.8% in the absence of chloride. Although no in-situ measurement of Eh was available, these results suggest that the Eh was lower in the chloride-containing system. Furthermore, for chloride concentrations of both 15 g/L (Figure 2B) and 100 g/L (Figure 2C), a high sulphur content (18%–20%) was noted in the 10 min residue, consistent with covellite preferentially forming elemental sulphur upon dissolution in a chloride environment. In comparison, the maximum amount of sulphur formed in the absence of chloride was ~2% (Figure 2C).

Low-temperature studies of chalcopyrite dissolution have indicated no evidence for the (stable) formation of chalcocite. During low-temperature bioleaching of chalcopyrite, XANES and Raman spectroscopy suggested the formation of a “covellite-like” phase, although with crystallite size too small for XRD identification; there was no evidence for chalcocite formation even though the Eh was maintained at relatively low values of 350–480 mV [81]. The mixed potential provided by the Fe<sup>2+</sup>/Fe<sup>3+</sup> couple was also demonstrated by Yang et al. [82] to facilitate chalcopyrite leaching via the formation of a chalcocite intermediate which it was claimed to be rapidly oxidised by Fe<sup>3+</sup> ions and hence not detected by XRD analysis or Raman spectroscopy. That chalcocite is not formed even in chloride-containing solutions at sufficiently high oxidation-reduction potential is consistent with various studies, e.g., [83]; Gao et al. [84] noted that covellite is preferentially formed under oxidising conditions.

Covellite is indicated to be the most stable copper sulphide, being the end product derived from various copper sulphide minerals as discussed by Muszer et al. [17]. These researchers also demonstrated covellite persists as an intermediate product during pressure oxidation of a mixed sulphide concentrate in 120 g/L sulphuric acid at 180 °C with oxygen partial pressure of 5 atm for beyond 4 h, albeit at a moderate stirrer speed of 400 rpm, similar to the finding of Jiang et al. [15]. Furthermore, covellinisation of copper sulphide minerals does not hinder copper extraction at temperatures of 160 °C and below: using a synchrotron technique, Majuste et al. [85] detected the presence of covellite (CuS) during in-situ dissolution studies of chalcopyrite in acidic ferric sulphate media at 100–200 °C under static (as opposed to flow-through) cell conditions whereby redox potential of the electrolyte solution progressively dropped from its initial value of 750 mV (SHE) due to ferric iron consumption. These findings are consistent with the conclusion of Velásquez-Yévenes et al. [86] that below a solution potential of 540 mV (versus Ag/AgCl) the rate of copper dissolution decreases, albeit at 35 °C, and only once the potential increased above 580 mV did it increase significantly. It was also noted by these researchers that at lower potentials covellite and/or chalcocite formed on the chalcopyrite surface. In the current study, chalcocite may have formed as an intermediate, but its presence was too brief to detect in the earliest samples taken, i.e., after 2.5 min. Acquisition of a sample

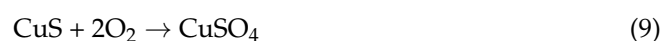
within seconds of the introduction of a low, controlled oxygen partial pressure or after injection of a controlled ratio of ferric and ferrous chlorides to target a specific liquor Eh could potentially demonstrate whether chalcocite is formed as a stable intermediate at the temperatures studied here. Here, the application of in-situ techniques may be beneficial for the identification of transient changes during chalcopyrite leaching.

Cai et al. [58] proposed a mechanism for the reaction of covellite with hydrochloric acid at a low temperature of 100 °C under non-oxidising conditions in which chloride is able to replace sulphide in the covellite structure with the subsequent dissolution of the Cl-covellite to generate elemental sulphur according to equations similar to:

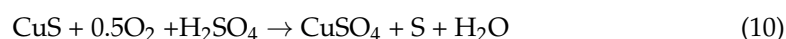


Peters and Loewen [87] suggested a second simultaneous mechanism for the reaction of covellite whereby sulphate is directly produced whereas, elemental sulphur where formed was shown to be stable to perchlorate oxidation at 125 °C.

The mechanism for the direct oxidation of covellite is given by the following equation:



This reaction appears relevant to the current study since covellite was also detected in early residue samples (9.8% after 2.5 min) when no chloride was added to the system (see Figure 2C); subsequent samples contained only small amounts of sulphur (~2% as noted previously). In comparison, the 2.5 min sample obtained with 1.4 M Na<sub>2</sub>SO<sub>4</sub> addition contained 7.2% covellite; however, subsequent samples did not contain any detectable sulphur. The premise that a similar proportion of sulphur relative to covellite is produced when no chloride is added and then subsequently oxidised to sulphate is also inconsistent with the data of Corriou and Kikindai [88] who indicated that at a temperature of 200 °C the oxidation of sulphur occurs at similar rates in sulphate- and chloride-based systems. It, therefore, appears the presence of chloride strongly favours the reaction of covellite at high temperature to generate sulphur (Figure 2B,D), and for which the overall simplified reaction can be expressed as:



The data for the tests presented in Figure 2 and others in this study are consistent with the covellite exclusively being the primary intermediate in the oxidation of chalcopyrite when chloride is present. However, when chloride is absent, covellite is only present during the first few minutes of the reaction as seen in Figure 2C. While not detected after 5 min for the reaction conducted at 230 °C, it was present in the 2.5 min sample at 245 °C (see Section 4.5.4). Thus, covellite is produced as an intermediate and reacted rapidly under all conditions studied here.

That covellite dissolution when chloride is absent appears to occur via Equation (9) would suggest this is rapid compared with the oxidation of chalcopyrite to covellite given that only trace amounts of covellite were detected. Alternatively, it could indicate that covellite is not significantly formed as an intermediate. Thus, when the generation of covellite is minor, the initial dissolution of chalcopyrite can be simply represented by the (net) equation:



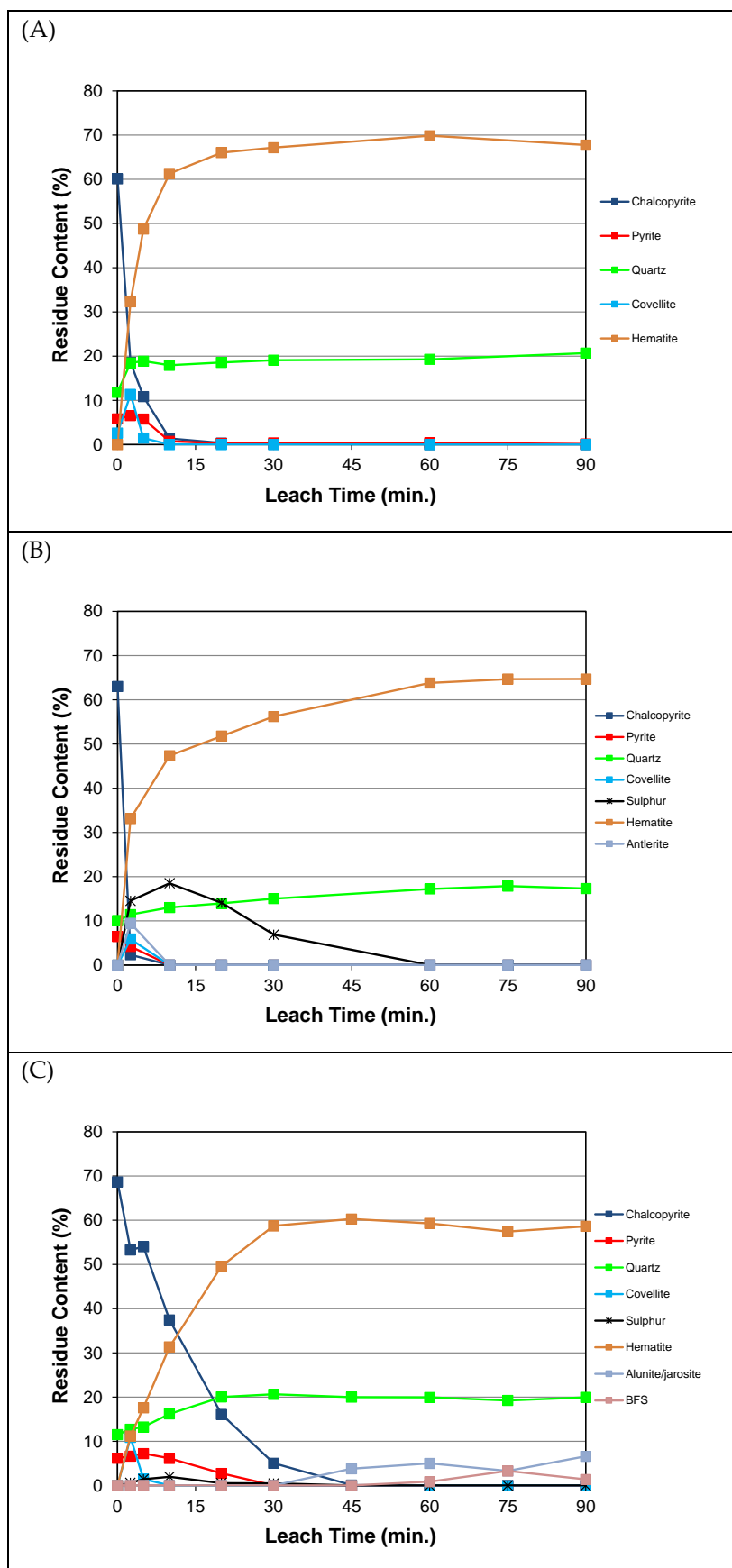
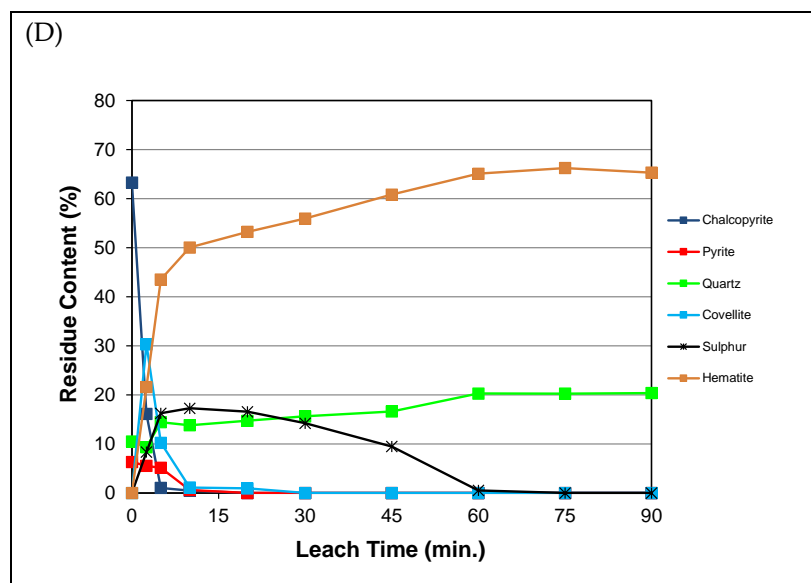


Figure 2. Cont.



**Figure 2.** Mineralogy of the leach residues obtained during the leaching of chalcopyrite concentrate ( $P_{100} - 45 \mu\text{m}$ ) under pressure oxidation conditions ( $220 \text{ }^\circ\text{C}$ ,  $700 \text{ kPa O}_2$ ) for various pulp density (PD as %  $w/w$ ) and chloride concentrations (Cl as g/L) (A) PD 10 and Cl 0, (B) PD 10 and Cl 15, (C) PD 20 and Cl 0, and (D) PD 20 and Cl 15. Chloride added as NaCl.

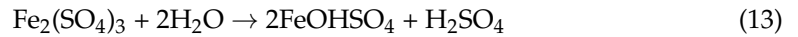
Dissolved iron was oxidised and hydrolysed to form a variety of residue minerals depending upon the conditions under which the chalcopyrite is leached. At 10%  $w/w$  pulp density, and with no chloride addition, hematite was rapidly formed and its content remained stable in the leach residue (see Figure 2A) since free acidity remained below the “break point” value, i.e., the critical value at the temperature of interest above which iron is hydrolysed to form basic iron sulphates, viz., the transition between low- and high-sulphur containing iron hydrolysis residues. This term was discussed in the review of Whittington and Muir [89] and can be traced back to the work of Tozawa and Sasaki [90] and prior to that, the rapid change in sulphur content of iron hydrolysis residues as a function of free acidity identified by Umetsu et al. [91].

Hematite formation was slower when the pulp density was increased to 20%  $w/w$  as the chalcopyrite reacted more slowly, but still constituted the dominant iron-containing phase (see Figure 2C). Once the acidity had increased sufficiently, and specifically, this refers to the in-situ proton activity rather than the titrated free acidity, small amounts of natrojarosite and basic ferric sulphate were formed including via the dissolution of a fraction of the hematite previously precipitated.

In the presence of 15 g/L added chloride, faster leaching of chalcopyrite is seen in Figure 2B,D, leading to a more rapid increase in copper sulphate concentration which buffers the “at temperature” acidity. Furthermore, the lower free acidity values during the periods when elemental sulphur is present meant the “break point” acidity value was approached more slowly during these experiments and even at 20%  $w/w$  pulp density there was insufficient time for hematite conversion to basic iron sulphates to occur.

The buffering effect of metal sulphates in controlling “at temperature” acidity as described by Tozawa and Sasaki [90] has rarely been considered. Cheng and Demopoulos [92] examined the impact of zinc sulphate upon iron hydrolysis to establish reaction kinetics with the aim of being able to shorten the Akita process retention time below 3 h. More recently, Fleuriault et al. [7] examined mixtures of copper sulphate, ferrous or ferric sulphate and sulphuric to recreate the matrix compositions that arise from the pressure oxidation of copper sulphides. The “break point” acidity was shown to increase with increasing copper sulphate concentration. Increasing initial acid concentration was often associated with a drop between the initial and final free acidity of the solution, consistent with complete

oxidation of the ferrous iron but incomplete hydrolysis to form residues dominated by basic ferric sulphate (otherwise the free acidity would remain the same):



In the current study, the copper concentrations generated at pulp densities of 10% *w/w* and 20% *w/w* were typically ~30 g/L and ~65 g/L, respectively. The buffering of acidity by the dissolved copper sulphate enabled free acid levels of ~45 g/L and ~95 g/L, respectively, to be achieved in the absence of additional upfront sulphuric acid at low-to-moderate chloride levels (3–15 g/L), with the minor formation of basic ferric sulphate minerals. Typically, the mineral formed was a mixed (natro)alunite/jarosite phase (with low aluminium content) that only accounted for a small fraction of the iron in the residue. In comparison, the up-front addition of sulphuric acid was sufficient to ensure the “break point” acidity was exceeded and this is discussed further in Section 4.5.3.

#### 4.5.2. Effects of Added Chloride and Oxygen Partial Pressure

As previously noted in Figure 2C, when chloride is absent the amount of elemental sulphur detected in the residues was low,  $\leq 2\%$ . In comparison, the addition of even a small amount of chloride (3 g/L) significantly increases the amount of elemental sulphur formed (Figure 3A). This is consistent with partial oxidation of the covellite intermediate according to reaction (10). Increasing the chloride concentration to 15 g/L enhanced the contribution of this reaction to the overall mechanism (Figures 2D and 3D). Furthermore, it is known that the presence of various acids and salts, i.e., NaCl, HCl, Na<sub>2</sub>SO<sub>4</sub>, NaHSO<sub>4</sub> and H<sub>2</sub>SO<sub>4</sub>, with increasing concentrations, results in a reduction in the rate of sulphur oxidation at 200 °C [88]; a similar effect of increasing acid concentration was found at lower temperatures, 105–140 °C, by Peters and Loewen [87]. This, however, is inconsistent with the rate of sulphur oxidation when the chloride addition is 100 g/L (Figure 3B). Although not proven here, this behaviour is consistent with changes in the size of sulphur droplets, and thus their surface area, as a function of chloride concentration in the present systems. Corriou and Kikindai [88] concluded that only “liquid” sulphur is oxidised. While this conclusion is not strictly correct, the rate of aqueous oxidation of (solid) sulphur at 90 °C is extremely slow and only increases appreciably above its melting point [93]. Once formed, solid sulphur is relatively inert and has been detected on chalcopyrite electrodes at a high applied potential, 1.0 V SHE [94].

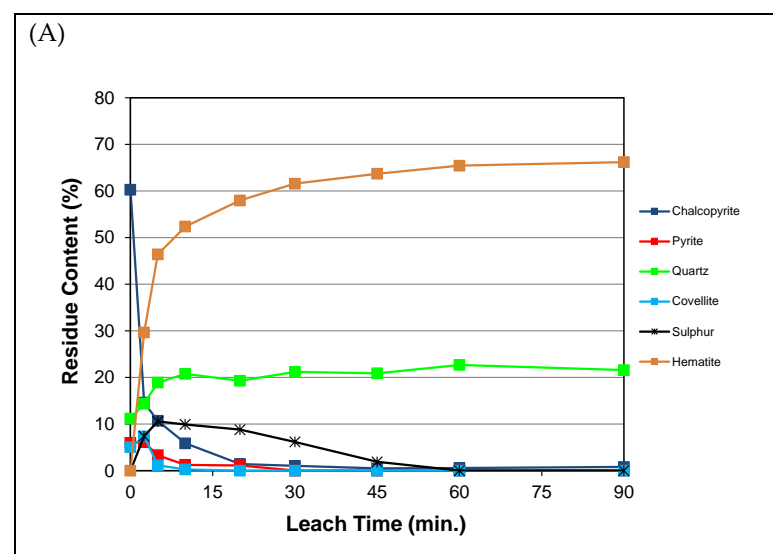


Figure 3. Cont.

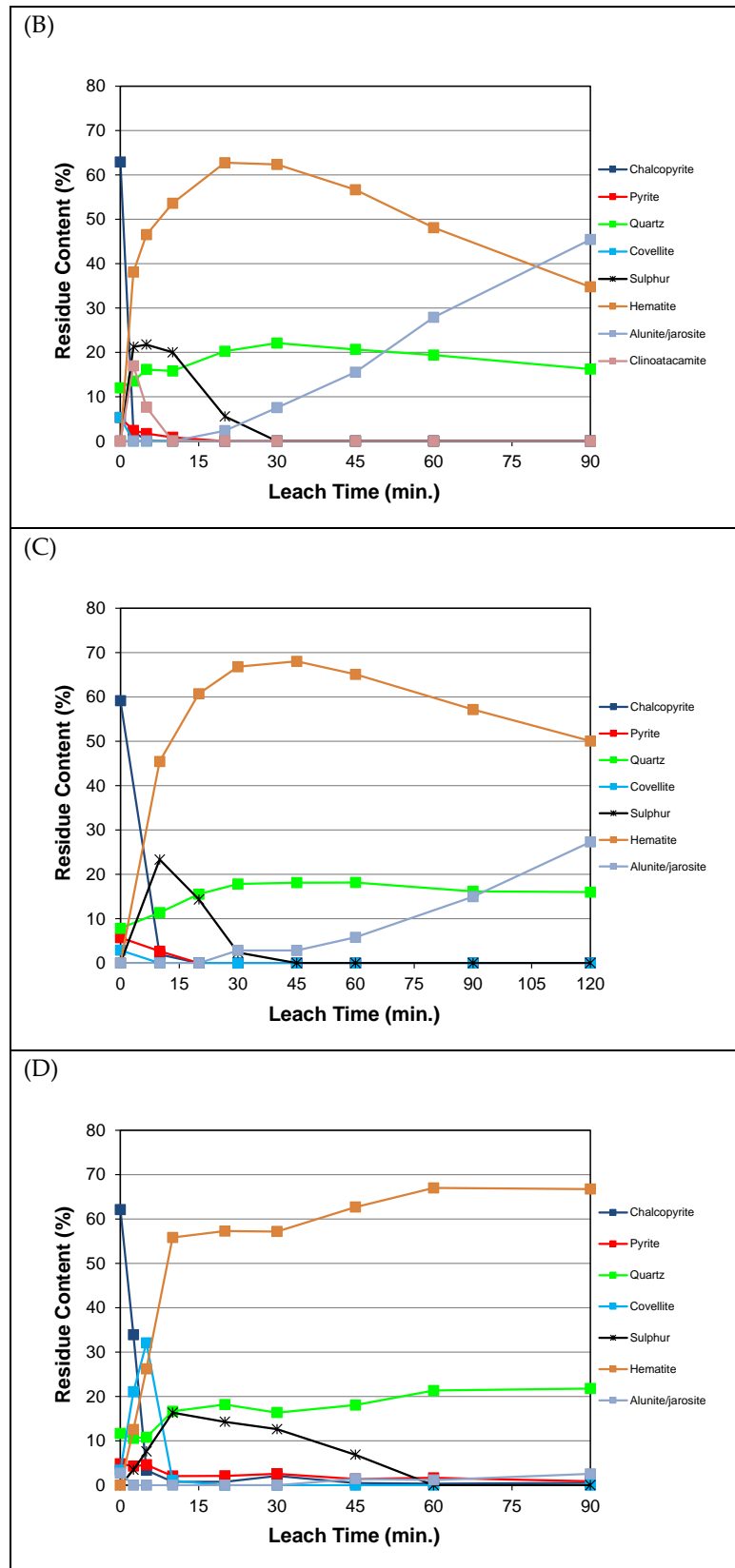


Figure 3. Mineralogy of the leach residues obtained during the leaching of chalcopyrite concentrate ( $P_{100} - 45 \mu\text{m}$ ) under pressure oxidation conditions ( $220 \text{ }^\circ\text{C}$ ,  $700 \text{ kPa O}_2$ ,  $20\% w/w$  pulp density) for various and chloride concentrations (Cl as g/L) (A) Cl 3, (B) Cl 100, and (C) Cl 100 (repeat). An oxygen partial pressure of  $100 \text{ kPa}$  was used for (D) Cl 15. Chloride was added as NaCl.

The slower oxidation of elemental sulphur at the lower chloride additions ensures the dominant iron-containing residue is hematite (even though many of the experimental systems contain added sodium). As the bulk of the iron is dissolved and re-precipitated within 10 min, the free acidity was not sufficiently high to favour the formation of basic iron sulphates. It was only once free acidity increased beyond 60 g/L that the hematite was dissolved and with increasing free acid levels was subsequently re-precipitated as either natrojarosite and/or basic ferric sulphate. Even after 90 min, it was notable that the solid-state equilibrium between hematite and natrojarosite had not been established (Figure 3B); an earlier repeat experiment although giving a somewhat different distribution of mineral phases confirmed this finding (Figure 3C). This is also consistent with the studies of King et al. [33,34] who found the sulphate content of residues produced from the pressure oxidation of copper concentrates at temperatures of 200–220 °C increased between 1 h and 3 h reaction time. They also noted the sulphate contents of residues formed at 220 °C were greater than of those formed at 200 °C. A similar result was found in the present study where the sulphur content of residues even after 90 min increased from 1.2 to 1.3 to 3.9% *w/w* at temperatures of 220, 230 and 245 °C, respectively, when 15 g/L chloride was added. Here, however, the absence of natrojarosite in the residues formed at 220 and 230 °C suggests most of the sulphate is associated with hematite and is either encapsulated within the structure and/or adsorbed onto the surface of this phase. In comparison with the present study, Ruiz et al. [95] found the sulphur content of hematite formed at temperatures between 180–220 °C decreased with increasing temperature but was somewhat higher, 1.9% *w/w*, for hematite formed at 220 °C.

The detection of clinoatacamite (see Figure 3B) was noted when the chloride addition was 100 g/L and for samples taken between 2.5–5 min. Its presence (and that of antlerite when the chloride addition was 15 g/L and pulp density was 10% *w/w* as shown in Figure 2B) corresponds to low free acidity in the leach liquors. The formation of basic copper salts is discussed further in Section 4.5.8.

Reducing the oxygen partial pressure to 100 kPa reduced the rate of chalcopyrite oxidation and enhanced the covellite content (~32%) in the 5 min residue sample (Figure 3D). Although the data suggest the reduction in reaction rate is not proportional to the oxygen partial pressure, this may also reflect the variation in the induction period required to fully saturate the leach liquor with dissolved oxygen at the different oxygen pressures. It was, however, expected that the systems were saturated in oxygen after several minutes. Examination of the data also indicates that the rate at which elemental sulphur was oxidised was similar at the lower oxygen partial pressure employed (see Figures 2D and 3D), whereas Habashi and Bauer [93] proposed a rate proportional to  $pO_2^{3/2}$  at temperatures between 130 °C and 170 °C. In comparison, Corriou and Kikindai [88] reported that sulphur is less reactive at temperatures between 175 °C and 230 °C and the reaction rate is proportional to  $pO_2/(1 + c pO_2)$  at 200 °C, where  $pO_2$  is the oxygen partial pressure and  $c$  is a constant.

#### 4.5.3. Effect of Added Sulphuric Acid

The up-front addition of sulphuric acid to the leach pulp (which in application terms is equivalent to the recycling of acidic liquor to the leaching stage) had a significant impact on the leach residue composition as indicated in Figure 4. As noted previously, the addition of acid alone, i.e., with no chloride, slows the leaching process and this is confirmed by the slower disappearance of chalcopyrite (Figure 4A,C); this also correlates with the extraction of copper [1]. It was also noted by Antonijević and Bogdanović [96] that chalcopyrite leaching becomes slower with decreasing pH, which was ascribed to the enhanced generation of an iron-deficient passivation layer at the surface of the chalcopyrite particle as it leached; a similar result was reported by Córdoba et al. [97]. This conclusion is not contradicted by the results of this, and the previous study [1]. In comparison, the recent study of Jiang et al. [15] reported chalcopyrite leaching (with no added acid) conducted at 160–180 °C, typically with a total pressure of 1.5 MPa (including partial pressure of oxygen), no suggestion for phases that could inhibit the reaction. This conclusion was based upon

XPS analysis of leach residues generated when the agitation speed in their reactor was 700 rpm (or greater); at lower agitation speeds the reaction of chalcopyrite was slower and significant amounts of covellite intermediate could be detected.

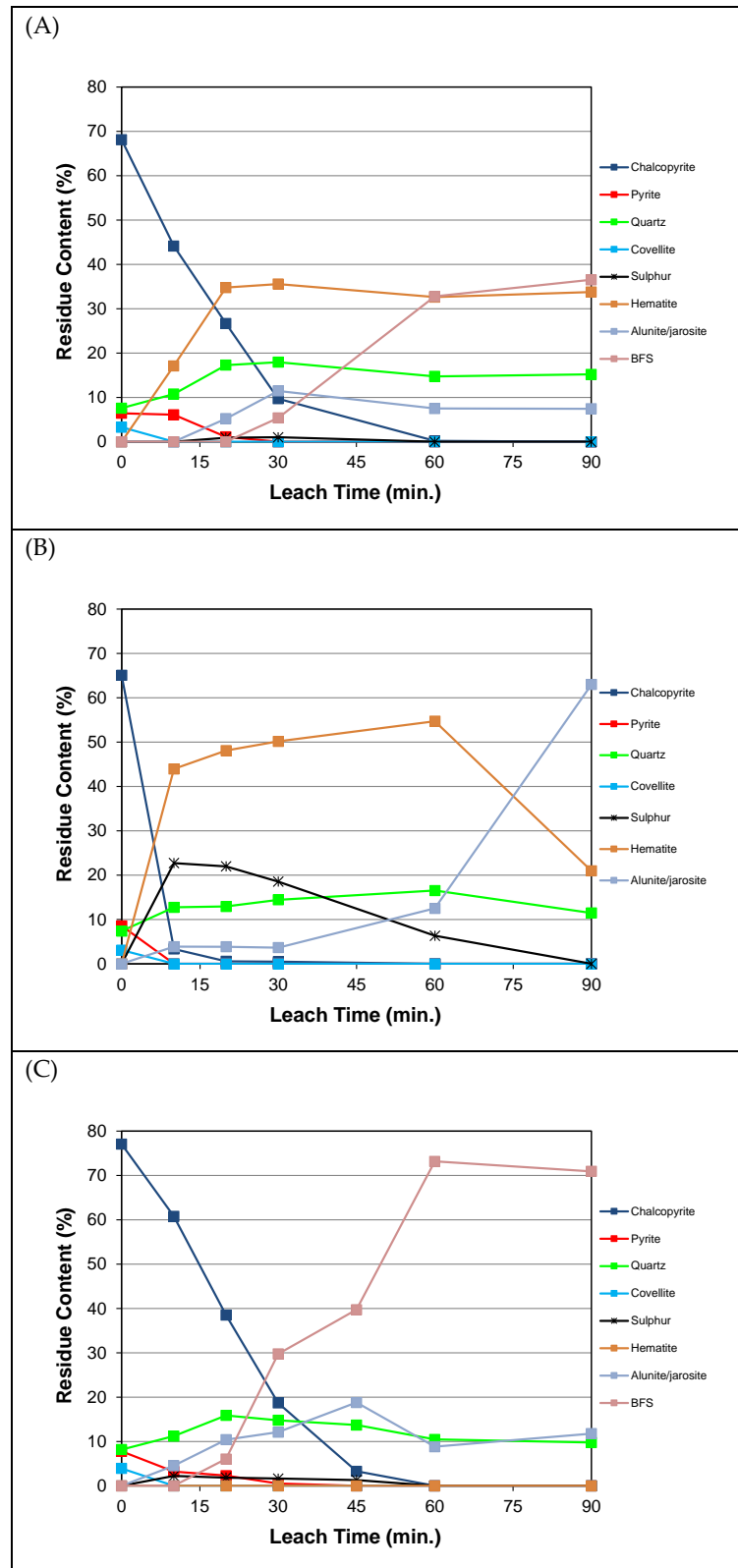
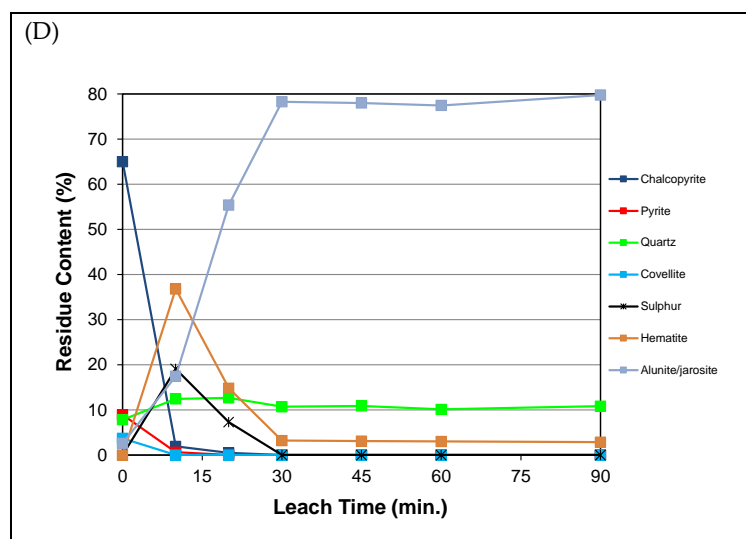


Figure 4. Cont.



**Figure 4.** Mineralogy of the leach residues obtained during the leaching of chalcopyrite concentrate ( $P_{100} - 45 \mu\text{m}$ ) under pressure oxidation conditions ( $220 \text{ }^\circ\text{C}$ ,  $700 \text{ kPa O}_2$ ,  $20\% w/w$  pulp density) for various chloride (Cl as g/L) and acid concentrations (A as g/L) (A) Cl 0 and A 30, (B) Cl 15 and A 30, (C) Cl 0 and A 100, and (D) Cl 100 and A 100. Chloride added as NaCl.

The passivation of chalcopyrite surfaces is not considered from this study to impact the chalcopyrite leaching in the presence of added chloride as over 95% copper extractions were achieved within 10 min even when acid, either 30 g/L or 100 g/L, was added up-front [1]; it is also noted that the stirrer speeds greater than 600–700 rpm were employed. The rapid copper extractions are consistent with the rapid disappearance of chalcopyrite in leach residues though, potentially passivating phases that include covellite, sulphur and hematite were formed. It was proposed in the previously [1] that a surface chloride-mediated rate-determining step ensures that chalcopyrite leaching is enhanced in the presence of chloride.

With increasing initial acid concentration, the formation of basic iron sulphate,  $\text{Fe}(\text{OH})\text{SO}_4$ , is also enhanced, which is undesirable from an environmental perspective and because it can interfere with downstream processing, e.g., [98]. The co-presence of chloride, as sodium chloride, promotes the formation of natrojarosite at the expense of basic ferric sulphate, but this is also undesirable due to its environmental instability [99], and because of its higher volume as an iron-containing residue than hematite. The formation of this phase was evident when high acid and high chloride additions were employed, Figure 4D, as the final residue consisted of just over 80% sodium jarosite (unit cell parameters  $a = 7.318 \text{ \AA}$ ,  $c = 16.609 \text{ \AA}$ ). While the generation of copper sulphate during tests for which moderate up-front sulphuric acid was added, i.e., 30 g/L, provided some initial buffering of the acidity, this was insufficient to hinder the formation of basic iron sulphate phases within the timeframe of the experiments.

#### 4.5.4. Effects of Temperature

Although not relevant to the current feed material, if the concentrate being pre-treated by pressure oxidation was a copper-gold one, the elimination of the elemental sulphur would be critical to optimise subsequent gold recovery from the leach residue using conventional cyanidation, e.g., [30]. While copper extraction in the present study exceeded 98% at times between 10 and 30 min during pressure oxidation at  $220 \text{ }^\circ\text{C}$ , sulphur oxidation was not complete for times up to 60 min when  $\geq 3 \text{ g/L}$  chloride was added to the leaching system. Therefore, experiments to enhance the rate of sulphur oxidation and ensure rapid copper extraction were conducted.

Collins et al. [30] identified increasing reaction temperature as leading to improved subsequent gold recovery; higher temperatures were also trialled in this study. The impacts

upon residue mineralogy are shown in Figure 5. For a moderate chloride concentration of 15 g/L and pulp density of 20% *w/w*, elemental sulphur was oxidised for around 30 min at 230 °C (Figure 5A). At 245 °C, a trace amount of elemental sulphur, ca. 0.5%, was detected after 5 min but not after that time (Figure 5B). Interestingly, the residue taken at 2.5 min had a high covellite content, ~38%, though the elemental sulphur content was below the XRD detection limit. This suggests that the covellite oxidation mechanism changes with temperature, and is increasingly dominated by reaction (9), although enhanced oxidation of elemental sulphur (if formed as an intermediate) is also expected to occur at higher temperatures [93].

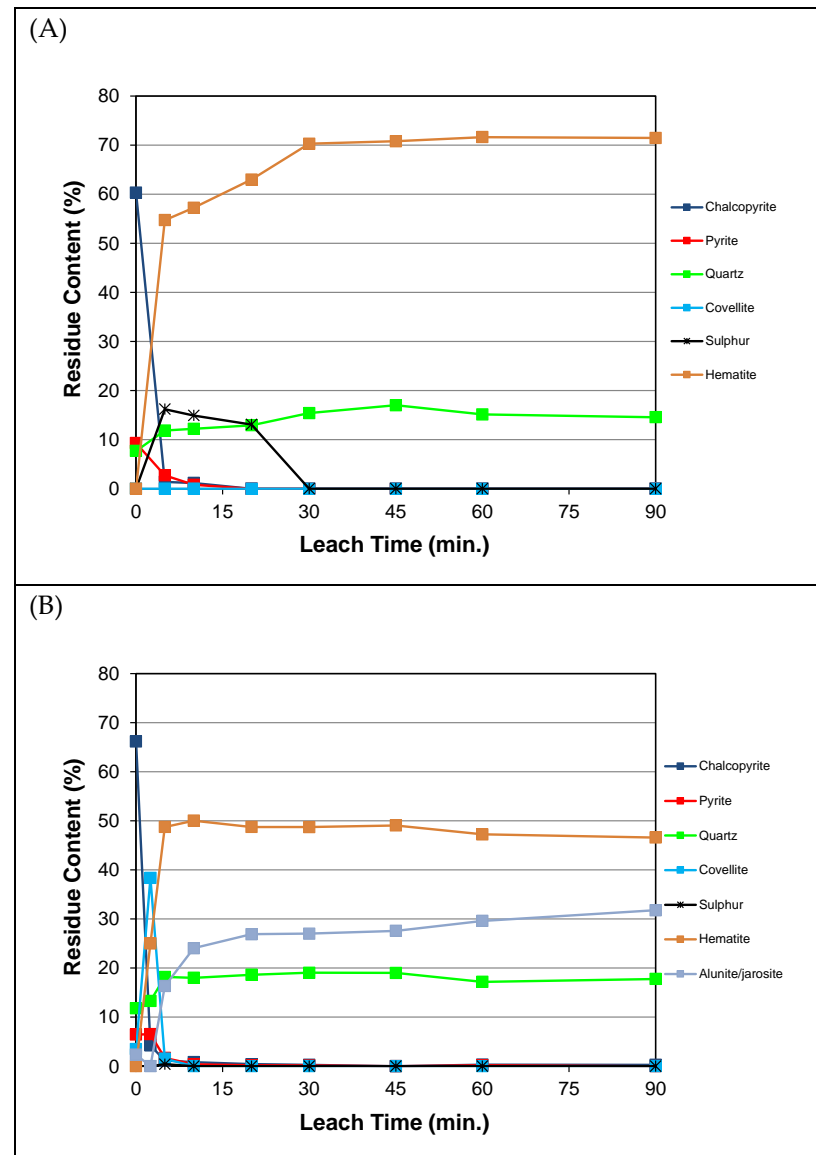


**Figure 5.** Mineralogy of the leach residues obtained during the leaching of chalcopyrite concentrate ( $P_{100} - 45 \mu\text{m}$ ) under pressure oxidation conditions (700 kPa  $\text{O}_2$ , 20% *w/w* pulp density, 15 g/L chloride added as NaCl) at higher temperatures (A) 230 °C, and (B) 245 °C.

At 245 °C the significantly enhanced conversion of sulphide to sulphate with accompanying increase in free acidity is consistent with rapid iron oxidation and hydrolysis to form hematite and natrojarosite (Figure 5B). Here free acidity reached 70 g/L after 5 min, compared to 39 g/L and 8 g/L at temperatures of 230 °C and 220 °C, respectively [1]. Notably, also, copper extractions were ~98% after 5 min at both higher temperatures while

the free acidity was clearly above the “break point” value at 245 °C; this corresponded to the formation of significant sodium jarosite (unit cell parameters  $a = 7.303 \text{ \AA}$ ,  $c = 16.608 \text{ \AA}$ ) that tended to increase slightly in content as the free acidity rose to 87 g/L by the completion of the reaction. Conversely, it can be concluded that for experiments where natrojarosite was not formed in significant amounts, solid-state equilibrium was probably not reached at completion of the experiment.

#### 4.5.5. Co-Presence of Pyrite

The galvanic effect of pyrite upon the leaching of chalcopyrite is well documented [100], although based upon this and subsequent studies, e.g., [101,102], the presence of catalysts such as  $\text{Ag}^+$  ions can further enhance this effect. A recent study, however, suggests galvanic contact with pyrite only marginally increases the rate of chalcopyrite dissolution at 30 °C, and this is insufficient to explain the large increases reported at higher temperatures [103].

In the present study, chalcopyrite typically reacts more rapidly than pyrite. This is consistent with pyrite being more inert than chalcopyrite in the ‘galvanic series’. Given that pyrite may encapsulate chalcopyrite, the slower leaching of pyrite, if still present, is one possible explanation for trace amounts of copper being extracted toward the conclusion of the pressure oxidation experiments [1]; the co-precipitation of copper with hematite is another, as noted by Javed and Asselin [104].

#### 4.5.6. Hydrohematite Formation

Wolska [105] identified that mild dehydration of amorphous iron(III) hydroxide produced “hydrohematite” at 160–200 °C that still contained ~3%–4.5% of tightly held water and for which the ratio of the (104) to (113) reflections in the XRD pattern was lower compared with crystalline hematite. It has also been noted for hematite that the (hk0), (hk3) and (hk6) reflections for hematite can be sharper than the others suggesting an anisotropic crystallite size [106]; this was modelled in the current QXRD analyses. Furthermore, it was identified that fitting of the hematite XRD patterns was improved by decreasing the iron-to-oxygen ratio, consistent with the presence of hydroxide and/or water in the structure.

The estimated water content for hematite typically produced in this study was 3.7%, consistent with the values of 3%–4.5% from Wolska [105] who indicated that calcination to 1000 °C was required for complete water removal. Wolska [105] hypothesised that this tightly held water is in the form of  $\text{OH}^-$  partly replacing  $\text{O}^{2-}$  in the hematite structure, i.e., “hydrohematite”. With such a replacement, electrostatic neutrality is disturbed and to preserve this charge imbalance, Fe(III) deficient sites are created in the cation positions. This Fe(III) deficiency results in lower intensity peaks for all but the (113) reflection [105]. In the subsequent study of Stanjek and Schwertmann [107] on synthetic aluminium-substituted hematites, it was concluded that the intensity of the XRD peaks normalised to the (113) reflection could only be explained by the inclusion of structural  $\text{OH}^-$ .

From the study of Javed et al. [11], a comparison of XRD patterns indicated sharper hematite peaks when formed in chloride-containing process liquor, while the water content of the hematite from TGA analysis was  $3 \pm 1\%$ . In the presence of copper sulphate, the extent of iron precipitation increased, and this was suggested to be due to buffering of acidity by the additional sulphate. In comparison, for the current study, the hematite peaks were of similar width whether chloride was present or not while the (hk0), (hk3) and (hk6) reflections were modelled to be marginally sharper than the others. Modelling the iron occupancy to enable the best fit to the intensity of the (113) peak gave an estimated formula for the “hydrohematite” of  $\text{Fe}_{1.79}\text{O}_{2.38}(\text{OH})_{0.62}$  and hence water content of 3.7% (as noted previously), within the ranges indicated by Wolska [105] and Javed et al. [11].

The buffering of acidity in the presence of additional sulphate has been noted previously [1]. Here, the addition of 1.4 M  $\text{Na}_2\text{SO}_4$  when compared with no salt addition in concert with the  $\text{CuSO}_4$  generated during chalcopyrite leaching further buffered acidity

to achieve a lower final iron concentration of 2.3 g/L compared to 4.8 g/L, and hence marginally greater iron precipitation.

#### 4.5.7. Effects of Additional Aluminium and Hematite Seeding

Two tests were conducted where aluminium-containing materials were added into the chalcopyrite leaching system, one using aluminium sulphate and the other, gibbsite. For both tests, 15 g/L chloride addition again facilitated the formation of elemental sulphur that slowly oxidised during the reactions (Figure 6A,B). In both instances, the extra aluminium promoted the formation of a (natro)alunite/jarosite solid solution phase, and when more acid was generated due to hydrolysis of the aluminium sulphate, this led to greater dissolution of the hematite and enhanced (natro)alunite/jarosite formation (Figure 6A). Notably, natroalunite formation preferentially occurs during heating when aluminium sulphate is added and the content of this phase only increases marginally during sulphur oxidation until beyond 60 min when the dissolution of hematite and alunite with re-precipitation of mixed (natro)alunite/jarosite phases accelerates. This behaviour has also been noted for solids formed during batch, high-pressure acid leaching of nickel laterites [108]. It was notable here that the (natro)alunite-rich component remained essentially invariant in composition up to 45 min and that the increase in the amount of (natro)alunite/jarosite phases was due to the formation of natrojarosite. Estimation of the (natro)alunite/jarosite phase composition from the unit cell parameters during QXRD analysis using the model of Whittington [109] enabled good fits to the peak intensities. It was calculated that the fraction of iron in the residue associated with (natro)alunite/jarosite phases increased from ~5 to 52% between 60 and 90 min. In contrast, when the source of aluminium was gibbsite, the lower free acidity due to the dissolution of this phase meant that solid state equilibrium was approached more slowly (Figure 6B), and the calculated fraction of iron reporting to the alunite/jarosite phases only increased from 9 to 12% over the same time period. The XRD pattern indicated the presence of two distinctly different mixed (natro)alunite/jarosite phases in addition to a (natro)alunite-rich phase formed early during the reaction. A comparison of the two tests clearly indicates that the availability of soluble aluminium and its impact upon free acidity in the system also affects iron hydrolysis and hence the iron-containing phase(s) formed.

The impact of hematite seeding upon the residue mineralogy as shown in Figure 6C is consistent with the reported copper extraction kinetics in the presence of 15 g/L chloride [1]. Although the addition of hematite reduces the contents of other phases in the residue proportionately, the most significant impacts were upon the reactions of covellite and elemental sulphur. Here the later dissolution of covellite delays copper extraction while the oxidation of sulphur to form sulphuric acid lagged behind that for comparable tests. In both cases, the slower rate of oxygen mass transfer given the solids loading is higher (initially 26.8% *w/w* after hematite seeding) is the driving factor for these delays.

#### 4.5.8. Formation of Basic Copper Salts

It was previously reported that under low temperature, low acid, Activox<sup>®</sup> conditions, substantial amounts of antlerite,  $\text{Cu}_3(\text{OH})_4\text{SO}_4$ , and/or atacamite,  $\beta\text{-Cu}_2(\text{OH})_3\text{Cl}$ , could be formed as the sulphur formed was only slowly oxidised to sulphuric acid during the reactions [6]. The formation of basic copper sulphate salt(s) can be tailored to occur during chalcopyrite processing and has been applied in the CESL process [110]. A recent study by Hawker et al. [18] that employed chalcopyrite concentrate with various additions of hydrochloric acid and sodium chloride, and at temperatures between 120 and 200 °C, noted variable formation of a basic copper chloride; Byrne et al. [48] indicated the salt formed to be atacamite. Studies such as that of Cheng and Lawson [111] have noted copper extraction from covellite at 90 °C drops with time at low starting sulphuric acid concentration and this can only be explained by the consumption of acid to sufficiently low levels with the resultant formation of basic copper sulphate salt(s).

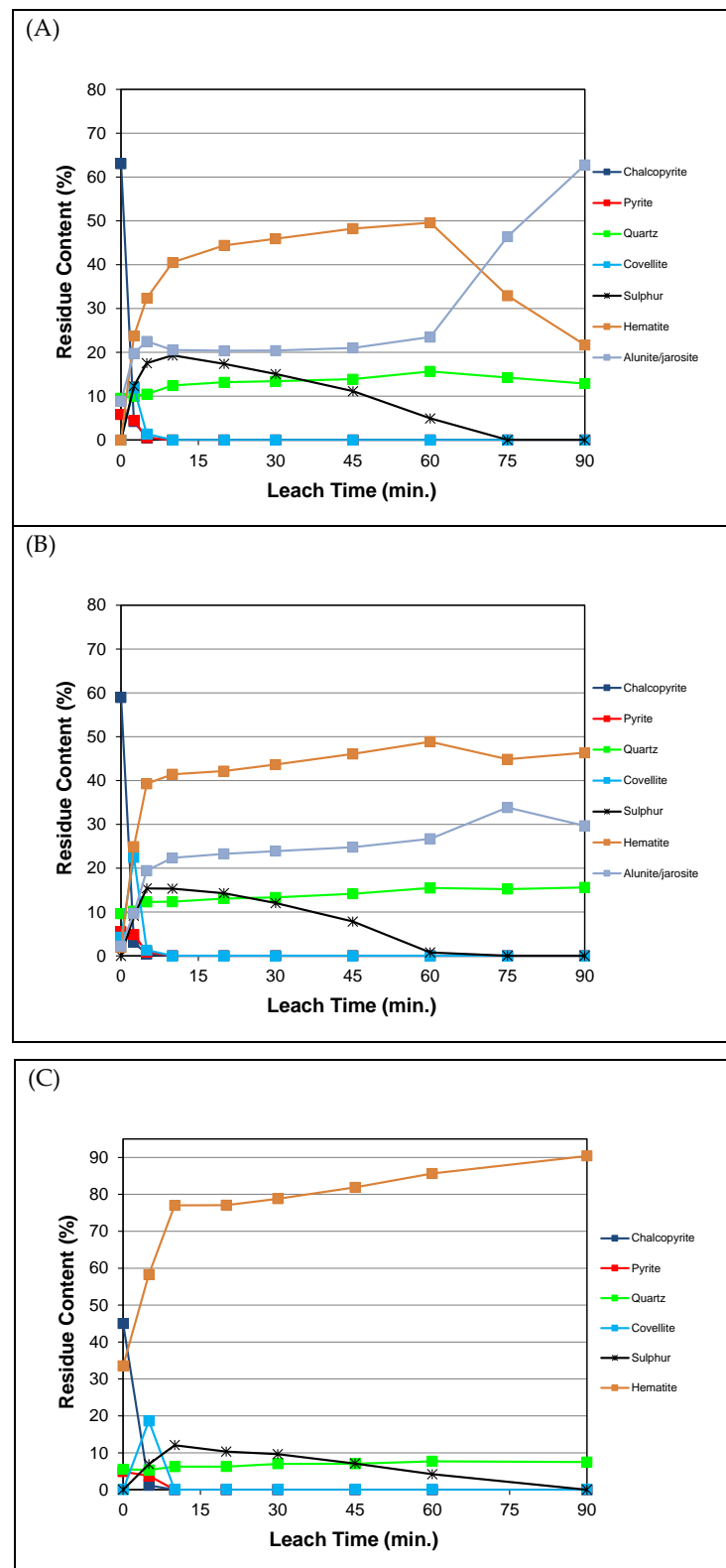


**Figure 6.** Mineralogy of the leach residues obtained during the leaching of chalcopyrite concentrate ( $P_{100} < 45 \mu\text{m}$ ) under pressure oxidation conditions (700 kPa  $\text{O}_2$ , 20%  $w/w$  pulp density, 15 g/L chloride added as NaCl) with the addition of (A) aluminium sulphate, (B) gibbsite and (C) hematite seeding.

As noted above, atacamite can be formed under Activox<sup>®</sup> conditions although the dominant basic copper mineral formed was antlerite [6]. The contribution of this phase to the XRD pattern of residue formed under such conditions is shown in Figure 7A. In

comparison, at high temperature (220 °C, 20% *w/w* pulp density, 700 kPa O<sub>2</sub> with 100 g/L Cl) the preferred basic copper phase formed was clinoatacamite ( $\gamma$ -Cu<sub>2</sub>(OH)<sub>3</sub>Cl) as shown in Figure 7C.

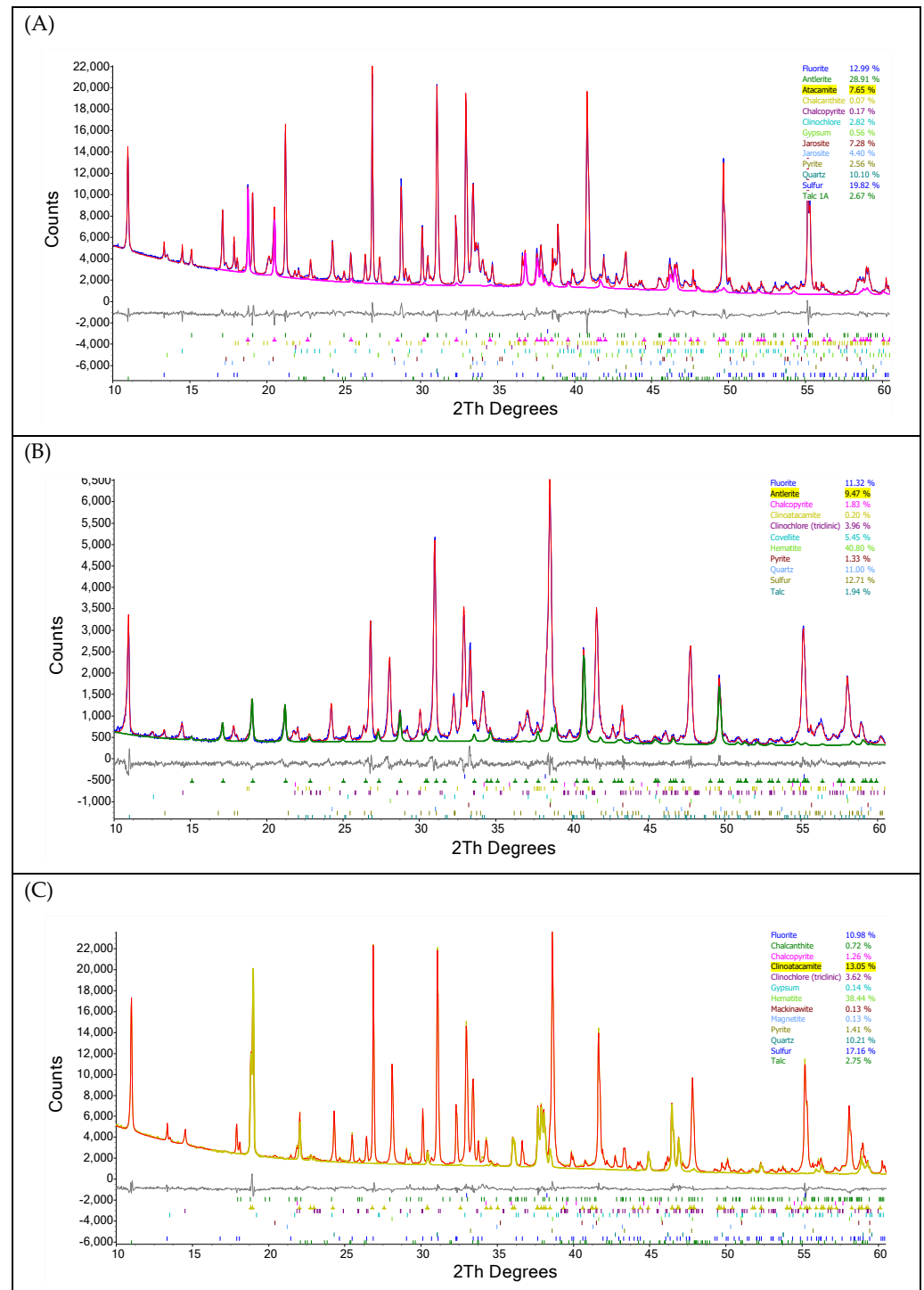


**Figure 7.** Rietveld analysis modelling of XRD patterns for residues obtained under pressure oxidation conditions: **(A)** 10% *w/w* pulp density, 108 °C, 700 kPa O<sub>2</sub> with 3 g/L Cu, 10 g/L Cl and 5 g/L H<sub>2</sub>SO<sub>4</sub> (45 min sample), **(B)** 10% *w/w* pulp density, 220 °C, 700 kPa O<sub>2</sub> with 15 g/L Cl (2.5 min sample), and **(C)** 20% *w/w* pulp density, 220 °C, 700 kPa O<sub>2</sub> with 100 g/L Cl (2.5 min sample). Contributions to the calculated patterns for the dominant basic copper salts are shown for clarity while calculated residual and peak positions for each phase are shown below the patterns.

In the present study, the preferential formation of elemental sulphur (as opposed to complete oxidation to form sulphuric acid) meant that low acid conditions existed when some of the early samples were taken. Antlerite for example, was also detected in the sample taken after 2.5 min for a test conducted with moderate chloride addition (220 °C, 10% *w/w* pulp density, 700 kPa O<sub>2</sub> with 15 g/L Cl) as shown in Figure 7B, but not when the pulp density was 20% *w/w* given the acid concentration after 2.5 min was much greater (3.0 g/L compared with 0.4 g/L); note that trace clinoatacamite was also present indicating that the chloride concentration of 15 g/L was too low compared to the sulphate concentration, ~34 g/L, for this phase to be preferentially formed. The formation of antlerite rather than brochantite, Cu<sub>4</sub>SO<sub>4</sub>(OH)<sub>6</sub>, was consistent with this phase becoming more stable with increasing temperature (and low pH). Comparisons of the relative stabilities of basic copper sulphates have been reported elsewhere, e.g., [112–114]; the relative stabilities of basic copper sulphate and basic copper chloride salts are examined in the studies of Woods and Garrels [115] and Pollard et al. [116]; others such as Scott [117] review the stability of basic copper chloride salts formed from bronze corrosion or used in pigments.

Of particular interest in the current tests was the formation of clinoatacamite, a polymorph of atacamite not detected in residues formed at lower temperatures [6]. Atacamite was found to be present in residues only provided the free acidity was low, typically <1 g/L. The chemical reaction for atacamite formation from chalcopyrite is given by the combination of Equations (27) and (24) (Section 4.5.9). Equation (27) predicts the formation of hematite and sulphur (with calculated sulphur to hematite mole ratio of 2.2) as seen in Figure 7C, with no acid formation whereas Equation (24) indicates the hydrolysis of copper is net acid generating. The detection of clinoatacamite can, therefore, only be explained if the acid is consumed by gangue minerals in the concentrate, e.g., clinocllore, which is reasonable given the liquor contained dissolved magnesium. Furthermore, only around one third of the extracted copper was hydrolysed, with corresponding reduction in chloride concentration from ~100 g/L to a calculated value of ~85 g/L; subsequently, the clinoatacamite dissolved between 2.5 and 10 min, increasing the copper concentration from ~40 to ~60 g/L during which elemental sulphur was oxidised to form acid. The dissolution of the clinoatacamite combined with on-going reaction with gangue minerals ensured the free acid concentration remained low during this period [1].

A similar explanation applies to the formation of antlerite in this study with the formation of hematite and sulphur prominent as shown in Figure 7B; here the calculated sulphur to hematite mole ratio is 1.6 which, after correction for the sulphur yet to be generated from the residual covellite (Equation (16)), increases to 1.8. These results suggest there is potential to generate stable basic copper salts under high temperature, alkaline pressure oxidation conditions. Several studies have confirmed that the chalcopyrite rest potential decreases with increasing pH and that the formation of iron- and copper-containing phases do not hinder oxidation at moderate potentials under alkaline conditions [118–120]; glycine leaching of chalcopyrite is also conducted under alkaline conditions [121].

Notably, high temperature is not necessarily required for clinoatacamite formation is that high temperature is not necessarily required for its formation [122] which has also been demonstrated to occur during the extraction of chalcopyrite under alkaline conditions at 80 °C [38]. However, while it is claimed further work is required to define the conditions under which the various atacamite polymorphs, including botallackite ( $\alpha$ -Cu<sub>2</sub>(OH)<sub>3</sub>Cl), e.g., [123], preferentially form, it is expected that clinoatacamite,  $\beta$ -Cu<sub>2</sub>(OH)<sub>3</sub>Cl, will be the most stable polymorph [124]. Prior to this study, clinoatacamite (incorrectly identified at the time as paratacamite) had been indicated to be the most stable basic copper chloride at room temperature [125]. Even earlier studies [115,126] reached a similar conclusion for acidic conditions, although Sharkey and Lewin [126] found atacamite was more stable than paratacamite at sufficiently high CuCl<sub>2</sub> concentrations. Subsequently, paratacamite is now no longer considered to be a true Cu<sub>2</sub>(OH)<sub>3</sub>Cl polymorph as it has a higher symmetry trigonal structure stabilised only by the inclusion of various isomorphous substituents for Cu<sup>2+</sup> such as Mg<sup>2+</sup>, Ni<sup>2+</sup> and Zn<sup>2+</sup>, e.g., [127–129].

Clinoatacamite can be prepared from atacamite under reflux conditions over a period of 6 days [130] and has a monoclinic crystal structure (space group  $P2_1/n$ ) as determined by several groups including Grice et al. [131]. In the present study, the unit cell parameters obtained for this phase from the Rietveld fit shown in Figure 7C are compared with various published values in Table 4.

**Table 4.** Summary of reported clinoatacamite unit cell parameters and values calculated from this study.

Unit Cell Parameter	Source					This Study
	[132]	[133]	[131]	[134]	[135] *	
a (Å)	6.166	6.157	6.144	6.164	6.1223	6.161
b (Å)	6.822	6.814	6.805	6.817	6.8346	6.823
c (Å)	9.120	9.105	9.112	9.114	9.1841	9.122
$\beta$ (°)	99.63	99.65	99.55	99.65	99.492	99.57

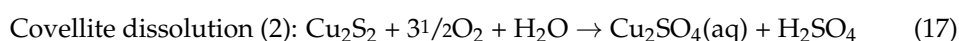
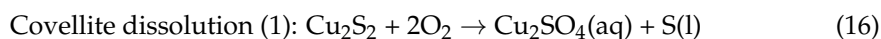
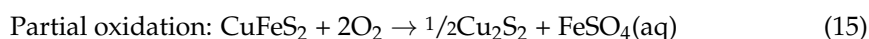
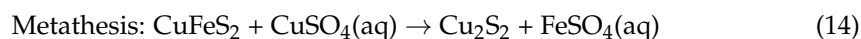
\* Note that this sample contains a small amount of Zn with corresponding formula  $\text{Cu}_{1.92}\text{Zn}_{0.06}(\text{OH})_3\text{Cl}_{1.92}$ .

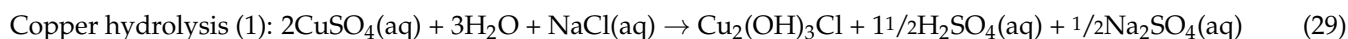
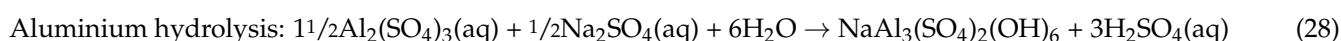
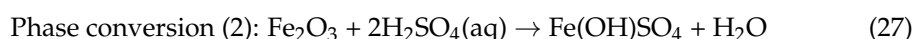
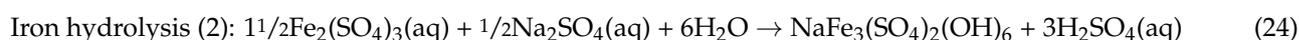
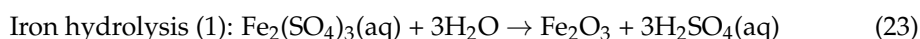
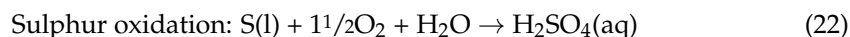
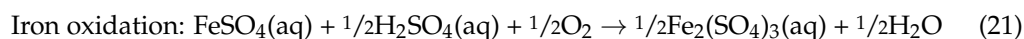
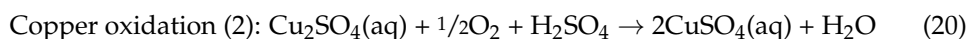
Returning to the polymorphs of  $\text{Cu}_2(\text{OH})_3\text{Cl}$ , clinoatacamite is regarded as being the end member of the Ostwald sequence for compounds with the formula  $\text{Cu}_2(\text{OH})_3\text{Cl}$  [124]. It is stated to have a Gibbs Free Energy of  $-1341.8$  kJ/mol compared with values for precursors in the Ostwald sequence of,  $-1339.2$  kJ/mol for atacamite and  $-1322.6$  kJ/mol for botallackite [136]. The study of Pollard et al. [125] concluded that each polymorph could be reproducibly synthesised. However, when formed, botallackite nucleates fastest and subsequently recrystallizes quickly under most conditions to a more stable polymorph; thus, the rarity of botallackite in nature. Increasing chloride concentration was found like Sharkey and Lewin [126] to inhibit the transformation of atacamite to clinoatacamite whereas increasing copper concentration and temperature promoted transformation.

Despite its higher stability, clinoatacamite is very rare in nature compared to atacamite [137]. In contrast, atacamite is found in a large number of world deposits forming as an oxidation product of copper minerals particularly under arid, saline conditions [138]. Notably, clinoatacamite is found together with atacamite in seafloor, hydrothermal sediments [139]; clearly, this is dictated by a combination of conditions that include the copper and chloride concentrations, and temperature. The implication of the current finding is that clinoatacamite will preferably form in geological settings under saline, hydrothermal conditions noting that the experimental conditions under which this phase formed here are likely to be extreme compared to natural environments, i.e., high copper and chloride (cf. seawater, 19.4 g/L). concentrations.

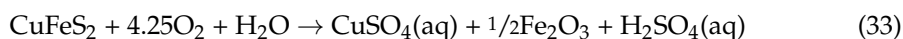
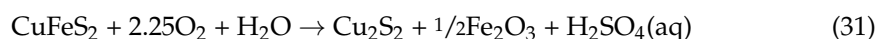
#### 4.5.9. Overview of Mineral Reactions

A summary of the reactions occurring in the various systems investigated and the products generated is given by chemical Equations (14)–(30); note here that covellite is represented by the formula  $\text{Cu}_2\text{S}_2$  rather than  $\text{CuS}$ , which is historically reported in the literature, though  $\text{Cu}_6\text{S}_6$  more accurately reflects the complex structural and electronic properties of this phase [14,140].





While several of these reactions are transient and others are slow on the timescale of the experiments conducted, the present and previous studies [1] demonstrate the scope for the manipulation of conditions to target specific products. Several such scenarios, e.g., the non-oxidative upgrading of copper concentrates and the recovery of basic copper salts, have been discussed previously. The selective combination of equations from above provides the following net Equations (31)–(33) for chalcopyrite leaching to target copper-rich streams and form hematite:



Based upon the last three equations, it is worth discussing further the behaviour of sulphur as impacted by the presence of chloride and temperature.

In the current tests the oxidation of sulphur content in the solids to soluble species, i.e., sulphate, provides an indication of how leaching reactions proceed in relation to the mineral phases present (Figure 8); less oxidised species such as thiosulphate may be present but were neither specifically analysed nor considered to be a significant component of the soluble sulphur-containing species under the conditions employed. While the extraction of copper is also informative for changes in mineralogy, this has been demonstrated to be decoupled from sulphur oxidation, as the snapshot of the reaction process is typically represented by a combination of reactions (32) and (33).

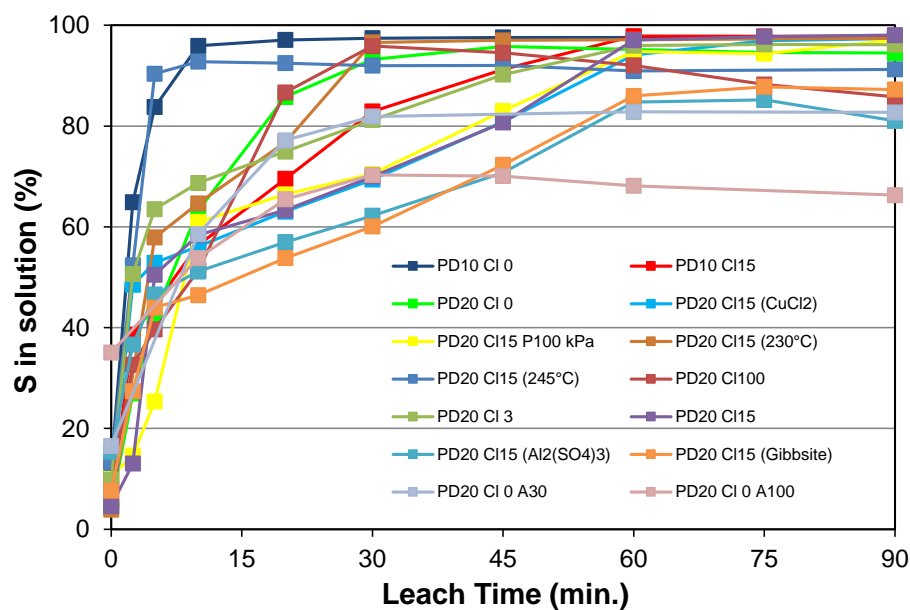


**Figure 8.** Change in dissolved sulphur-containing species concentrations during the leaching of chalcopyrite concentrate ( $P_{100} - 45 \mu\text{m}$ ) under pressure oxidation conditions (mostly  $220^\circ\text{C}$  and  $700 \text{ kPa O}_2$ ) at various pulp density (PD as %  $w/w$ ), chloride (Cl as g/L) concentration, and where indicated, acid (A as g/L) addition, temperature, pressure and other additives, i.e.,  $\text{Al}_2(\text{SO}_4)_3$  and gibbsite. Chloride normally added as sodium chloride; copper chloride ( $\text{CuCl}_2$ ) was added for one test.

With reference to Figure 8, the oxidation of sulphur is most rapid at 10%  $w/w$  pulp density in the absence of chloride. When chloride is present at 15 g/L, increasing the temperature to  $245^\circ\text{C}$  also enhances the rate of sulphur oxidation though, at the higher temperature, natrojarosite formation is favoured over hematite and increasing proportion of sulphur (as sulphate) reports to the residue as the system tends toward equilibrium. The significant formation of natrojarosite was only otherwise noted at  $220^\circ\text{C}$  when 100 g/L chloride was added (as NaCl) along with high upfront sulphuric acid (100 g/L) (see Figure 4D). Notably for these two tests, natrojarosite formation reduces the amount of dissolved sulphur by the conclusion of the reaction; as expected, this is also noted for other tests, e.g., where the addition of aluminium promotes the formation of (natro)alunite/jarosite phases and up-front addition of acid facilitates the formation of basic iron sulphate phases in preference to hematite.

Even though little elemental sulphur forms, the data in Figure 8 confirm the impact of increasing the pulp density to 20%  $w/w$  upon slowing the leaching of chalcopyrite (and pyrite) when no chloride is present. In contrast, the presence of low levels of chloride, here 3 g/L and above, hindered the oxidation of sulphur whereas the extraction of copper was enhanced [1]. The data in the figure also suggest there is a concentration of chloride ions, in the range 0–3 g/L, for which sulphate oxidation is best inhibited and above which, the oxidation rate then increases with increasing chloride concentration.

Decreasing the partial pressure of oxygen from 700 to 100 kPa had a most noticeable impact during the first 10 min during which the demand for oxygen is high. Thereafter the oxidation of sulphur occurs at a similar rate to that when the partial pressure is higher, again suggesting this reaction does not have a strong dependence on the oxygen partial pressure (with the equipment and under the conditions used in these tests).

The rapid initial increase in soluble sulphur species for a number of the reactions, more specifically those for which the subsequent increase is flatter and near linear (due to elemental sulphur oxidation) is typically consistent with the formation of covellite (and hematite) as given by Equation (31) with subsequent reaction of the covellite to generate elemental sulphur.

#### 4.5.10. Chemical Thermodynamics

The Gibbs Free Energy values at standard conditions for each of the reactions were calculated using data mostly reported in Lange's Handbook of Chemistry [141]; it is noted that NBS tables [142] could also have been used. Values for minerals not given in this resource were obtained from a range of sources as given in Table 5. The standard Gibbs Free Energy values,  $\Delta G_o$ , were calculated using Equation (34) and are given in Table 6.

$$\Delta G_o = \sum n_i \Delta G_o^i - \sum n_j \Delta G_o^j \quad (34)$$

**Table 5.** Thermodynamic quantities for minerals and hydrolysis products relevant to this study [114,115,143–151].

Mineral	$\Delta H_o$ (kJ/mol)	$S_o$ (J/mol K)	$\Delta G_o$ (kJ/mol)	References		
				$\Delta H_o$	$S_o$	$\Delta G_o$
Chalcopyrite	−194.9	124.9	−195.1			
Covellite	−54.6	67.4	−55.3	[143]	[143]	[143]
Hematite	−826.2	87.4	−744.4			
Natrojarosite	−3783.4	382.4	−3270.7	[144]	[145]	[146]
Natroalunite	−5132.0	321.1	−4622.4	[147]	[147]	[147]
Basic ferric sulphate	−1160.2	145.9	−1013.7	[148]	[148]	[148]
Antlerite	−1733.6	274.3	−1453.6	[114]	[114]	[114]
	−1750	263.5	−1467	[149]	[149]	[149]
Atacamite	−1672.7	335.6	−1339.9	[150]	[151]	[151]
	−1444			calc.		
Clinoatacamite			−1341.8			[115]

Here,  $i$  refers to the product species,  $j$  refers to the reactant species and  $n_i$  and  $n_j$  represent the stoichiometric coefficients of the reaction for the products and reactants, respectively. The value for  $\Delta G_o$  can also be calculated from the standard enthalpy,  $\Delta H_o$ , and entropy,  $S_o$ , values according to Equation (35) where  $i$ ,  $j$ ,  $n_i$ , and  $n_j$  have the same definitions as previous.

$$\Delta G_o = \left( \sum n_i \Delta H_o^i - \sum n_j \Delta H_o^j \right) - T \left( \sum n_i S_o^i - \sum n_j S_o^j \right) \quad (35)$$

These calculations provide a check of the internal consistency of the  $\Delta G_o$ ,  $\Delta H_o$  and  $S_o$  data and can be used to generate standard enthalpy and entropy values which are also reported in Table 6.

Each of the reactions described by Equations (14)–(27), (29) and (31)–(33) is indicated in Table 6 to proceed spontaneously under standard conditions. There are two exceptions: the first is the formation of antlerite, equation (30), and this is consistent with the study of Yoder et al. [113] who reported that this phase cannot be formed at room temperature from reactions between 0.05–1.2 M  $\text{CuSO}_4$  and 0.05–1.0 M  $\text{NaOH}$  solutions. The second is the formation of natroalunite, Equation (28) which typically employs temperatures above 100 °C for synthesis (e.g., [152]).

Every reaction in which oxidation of a solid, even if partial, occurs is strongly favoured and becomes increasingly so as the extent of oxidation increases, the two extremes being given by reactions (16) and (33). In comparison, most hydrolysis reactions (other than the formation of clinoatacamite) are weakly favoured under standard conditions. At higher temperatures these reactions become increasingly spontaneous and as their net entropy values are positive, typically several hundred J/mol K. Similarly, the transformations

of hematite to other iron-containing phases are weakly favoured and have positive net entropy values.

**Table 6.** Calculated standard Gibbs Free Energy, Enthalpy and Entropy values for reactions given by Equations (14)–(33).

Reaction	$\Delta H_o$ (kJ/mol) *	$S_o$ (J/mol K)	$\Delta G_o$ (kJ/mol) *
Metathesis (14)	−68.2	−28.2	−59.9
Chalcopyrite partial oxidation (15)	−858.1	−585.1	−683.7
Covellite dissolution with sulphur formation (16)	−656.7	−443.6	−534.0
Covellite dissolution with acid formation (17)	−1280	−801.0	−1041
Covellite complete dissolution (18)	−1580	−1114	−1248
Aqueous copper oxidation with Fe(III) (19)	−95.0	76.1	−117.5
Aqueous copper oxidation with O <sub>2</sub> (20)	−299.6	−312.9	−206.1
Aqueous iron oxidation with O <sub>2</sub> (21)	−102.3	−194.5	−44.3
Liquid sulphur oxidation (22)	−624.9	−392.5	−507.8
Hematite formation (23)	128.4	509.4	−23.7
Natrojarosite formation (24)	135.9	811.9	−82.6
Basic ferric sulphate formation (25)	83.4	371.8	−27.3
Hematite to natrojarosite conversion (26)	−37.7	31.8	−31.4
Hematite to basic ferric sulphate conversion (27)	38.5	234.1	−30.9
Natroalunite formation (28)	235.8	768.2	7.9
Clinoatacamite formation (29)	−548.9	268.5	−628.2
Antlerite formation (30) **	124.7 108.3	273.3 262.5	43.2 29.8
Chalcopyrite partial oxidation with hematite formation (31)	−896.2	−524.9	−739.8
Chalcopyrite partial oxidation with sulphur and hematite formation (32)	−1063	−724.5	−856.2
Complete chalcopyrite complete oxidation with hematite formation (33)	−1686	−1082	−1364

\* Values given are either per mol mineral/species reacted or per mol mineral generated (from aqueous components); \*\* Values calculated using the data of [114] and [149], respectively.

Although the metathesis reaction to form covellite, which occurs under non-oxidising conditions, is weakly favoured, the net entropy while being negative, is sufficiently small that the reaction remains spontaneous at high temperatures as described in Section 4.3. In contrast, the oxidative formation of (intermediate) covellite is suggested to drive the generation of soluble iron that is rapidly oxidised and hydrolysed to form hematite in the presence of added chloride.

The calculations presented in Table 6 indicated minor inconsistencies within the sets of data presented in Table 5, the most notable was the  $\Delta H_o$  value for atacamite calculated by Yoder et al. [150]. From the current calculations, a value of  $−1444$  kJ/mol is consistent with the  $\Delta G_o$  and  $S_o$  values reported by Puigdomenech and Taxén [151].

The redissolution of the basic copper salts formed, antlerite and clinoatacamite, occurs under near-equilibrium conditions and remains incomplete until sufficient sulphuric acid has been generated, as described in Section 4.5.8. These reactions are predicted from their equilibrium constant ( $\text{Log}K_r$ ) values of 8.29 and 7.34 [153] to be thermodynamically favoured; for the concentrations of dissolved copper and relevant, associated anions involved, complete dissolution of the basic copper salts is predicted to occur below pH values

of ~1.5 and ~1.0, respectively, though these values are only considered to be indicative given the equilibrium constants at high temperatures will be larger.

As a final comment, it has known that basic ferric sulphate becomes increasingly unstable in hydrometallurgical environments with decreasing temperature and this forms the basis for the “hot cure” process [98]. Furthermore, if water is present during the drying of leach residues containing this material, it can convert to butlerite,  $\text{Fe}(\text{OH})\text{SO}_4 \cdot 2\text{H}_2\text{O}$ ; hence the use of absolute ethanol for the final washing and milling of these residues. Notwithstanding, the prediction that the formation of basic ferric sulphate will be spontaneous remains valid given, as indicated above, the reaction has a positive net entropy.

## 5. Implications for Industrial Application

The impacts of chloride addition upon the leaching of chalcopyrite are long known and have found industrial development and application as described here and in part 1 of this study [1]. Furthermore, that chloride will be present in the processing of chalcopyrite in the future appears inevitable from examination of the literature, e.g., [154,155] and citations of this paper., due to the increasing scarcity of high-quality process water.

The presence of chloride during the high-temperature pressure oxidation of chalcopyrite concentrates is also beneficial and able to reduce the time required for optimum copper extraction by a factor of up to ~3 when compared to processing in the absence of chloride. Industrially, this should not be problematic as high-pressure acid leaching of nickel laterite ores using saline process water is commercially undertaken at the Ravensthorpe Nickel Operation; the materials of construction employed, e.g., Grade 17 titanium for the autoclave lining, provide excellent corrosion resistance in the presence of chloride. Notwithstanding, this author’s view is that the application of high-temperature, pressure oxidation to copper-containing concentrates will remain at a low level compared to low-temperature leaching approaches, e.g., heap (bio)leaching. It may find niche applications when treating beneficiated materials that contain penalty elements that prevent these from being processed using conventional smelting technologies. If so, the addition of chloride to the process will be beneficial, especially if conditions can be manipulated to reduce the oxidant requirement (and hence the subsequent requirement for neutralising reagents) and, enable the recovery of elemental sulphur as a valuable resource.

## 6. Conclusions

High temperature ( $\geq 220$  °C) pressure oxidation of a chalcopyrite concentrate was studied in batch mode normally employing 700 kPa  $\text{O}_2$  partial pressure. Pulp densities of either 10% or 20% *w/w* were employed and the impacts of dissolved chloride, sulphuric acid addition and other selected additives, each at varying concentrations or amounts, upon the copper extraction kinetics, the oxidation mechanisms, and the mineralogy of leach residues were examined.

The addition of chloride enhances the rate of copper extraction whereas up-front added sulphuric acid slows dissolution, especially in the absence of chloride. Chloride addition, however, favours an oxidation mechanism involving a covellite intermediate that reacts to liberate cupric ions and forms elemental sulphur. In the present study, covellite was the only intermediate copper sulphide phase detected; the formation of reduced copper sulphides such as chalcocite and digenite at best is transient but likely requires a higher ratio of dissolved to solid state copper based on the study of Chaudhari et al. [49] and/or less oxidising conditions, given that the oxidation of these phases occurs at a lower potential than covellite [156].

There is clear evidence from the decomposition of covellite for the effective decoupling of the copper oxidation/extraction and sulphate formation reactions. The elemental sulphur is slowly oxidised, generally resulting in a linear increase in free acidity to concentrations that should result in the formation of basic iron sulphate phases (in tests employing 20% *w/w* pulp density). Buffering of the “at temperature” acidity due to the high concentration

of cupric sulphate in the leach liquor results in the dominant iron-containing phase formed being hematite under many of the conditions studied.

The upfront addition of sulphuric acid at levels of 30 g/L, typical of the concentration of an acid recycle stream, was shown to increase free acidity above the “break point” value enhancing the formation of basic iron sulphate phases, normally natrojarosite in the presence of added NaCl and basic ferric sulphate in its absence. It is expected that a concentrate with lower copper and/or higher iron sulphide contents would be less forgiving and need to be pressure oxidised at lower pulp density to avoid basic iron sulphate formation, even in the absence of upfront sulphuric acid addition, unless the process liquor contained a metal sulphate buffer, e.g., Cu, Mg, at sufficient concentration. This approach, however, is not a panacea and further treatment of the residue may be required to reduce the basic iron sulphate content.

This study identified a range of other leach residue products, including intermediates, which can be formed including natroalunite derived from the addition of aluminium-containing materials, antlerite and clinoatacamite. Clinoatacamite, which has not previously been identified during the hydrometallurgical processing of copper minerals, is indicated to be the stable basic copper chloride polymorph formed under geohydrothermal conditions.

Thermodynamic analysis of the reactions proposed to occur from this study were generally consistent with these being spontaneous under standard conditions. Where this was not the case, elevating the temperature is sufficient to ensure reactions such as the formation of basic copper chloride salts and natroalunite occur.

**Funding:** The funding for some of the work reported here was provided by the Parker Centre for Integrated Hydrometallurgical Solutions.

**Data Availability Statement:** The data are not publicly available due to privacy issues.

**Acknowledgments:** This study is dedicated to the memory of David M. Muir as an acknowledgement of his significant achievements in the field of hydrometallurgy and his mentorship of the author during his time at CSIRO. The author also wishes to thank staff from the Analytical and Materials Characterisation group both past and present for their assistance in providing analytical and XRD measurements.

**Conflicts of Interest:** The author declares no conflict of interest.

## References

1. McDonald, R.G. The effects of chloride on the high temperature pressure oxidation of chalcopyrite: Some insights from batch tests—Part 1. Leach chemistry. *Minerals* **2023**, *13*, 1065. [[CrossRef](#)]
2. Marsden, J.O.; Brewer, R.E. Hydrometallurgical processing of copper concentrates by Phelps Dodge at the Bagdad Mine in Arizona. In *ALTA 2003 Copper 8 Conference*; ALTA Metallurgical Services: Melbourne, Australia, 2003; 17p.
3. Kuhn, M.C.; Arbiter, N.; Kling, H. Anacondas Arbiter process for copper. *Can. Min. Metall. Bull.* **1974**, *67*, 62–71.
4. Shin, D.; Ahn, J.; Lee, J. Kinetic study of copper leaching from chalcopyrite concentrate in alkaline glycine solution. *Hydrometallurgy* **2019**, *183*, 71–78. [[CrossRef](#)]
5. Khezri, M.; Rezai, B.; Abdollahzadeh, A.A.; Wilson, B.P.; Molaeinasab, M.; Lundström, M. Investigation into the effect of mechanical activation on the leaching of chalcopyrite in a glycine medium. *Hydrometallurgy* **2020**, *203*, 105492. [[CrossRef](#)]
6. McDonald, R.G.; Muir, D.M. Pressure oxidation leaching of chalcopyrite. Part I. Comparison of high and low temperature reaction kinetics and products. *Hydrometallurgy* **2007**, *86*, 191–205. [[CrossRef](#)]
7. Fleuriault, C.M.; Anderson, C.G.; Shuey, S. Iron phase control during pressure oxidation at elevated temperature. *Miner. Eng.* **2016**, *98*, 161–168. [[CrossRef](#)]
8. McDonald, R.G.; Muir, D.M. Pressure oxidation leaching of chalcopyrite Part, I.I. Comparison of medium temperature kinetics and products and effect of chloride ion. *Hydrometallurgy* **2007**, *86*, 206–220. [[CrossRef](#)]
9. Sahu, S.K.; Asselin, E. Characterization of residue generated during medium temperature leaching of chalcopyrite concentrate under CESL conditions. *Hydrometallurgy* **2011**, *110*, 107–114. [[CrossRef](#)]
10. Javed, T.; Abdul, B.; Ryan, D.; Raudsepp, M.; Asselin, E. Amorphous iron phases in medium temperature leach residues and associated metal loss. *Int. J. Miner. Process.* **2016**, *148*, 65–71. [[CrossRef](#)]
11. Javed, T.; Xie, M.; Asselin, E. Factors affecting hematite precipitation and characterization of the product from simulated sulphate-chloride solutions at 150 °C. *Hydrometallurgy* **2018**, *179*, 8–19. [[CrossRef](#)]

12. Drits, V.A.; Sakharov, B.A.; Manceau, A. Structure of ferroxhite as determined by simulation of X-ray diffraction curves. *Clay Miner.* **1993**, *28*, 209–222. [[CrossRef](#)]
13. Leach, D.L.; Braun, R.L. *Leaching of Primary Sulfide ores in Sulfuric Acid Solutions at Elevated Temperatures and Pressures*; No. UCRL-75899; CONF-750204-1; Lawrence Livermore Laboratory, California University: Livermore, CA, USA, 1974.
14. Chaiko, D.; Rocks, S.S.; Walters, T.; Asihene, S.; Eyzaguirre, C.; Klepper, R.; Baczek, F.; McMahon, G. The FLSmidth® rapid-oxidative leach (ROL) process Part II: A new chemical activation process for chalcopyrite. In *COM 2015, Conference of Metallurgists*; Canadian Institute of Mining, Metallurgy and Petroleum: Montreal, QC, Canada, 2015; 15p.
15. Jiang, L.; Leng, H.; Han, B. Dissolution and passivation mechanism of chalcopyrite during pressurized water leaching. *Minerals* **2023**, *13*, 996. [[CrossRef](#)]
16. Bartlett, R.W. Upgrading copper concentrate by hydrothermally converting chalcopyrite to digenite. *Metall. Trans. B Process Metall.* **1992**, *23*, 241–248. [[CrossRef](#)]
17. Muszer, A.; Wódka, J.; Chmielewski, T.; Matsuka, S. Covellinisation of copper sulphide minerals under pressure leaching conditions. *Hydrometallurgy* **2013**, *137*, 1–7. [[CrossRef](#)]
18. Hawker, W.; Byrne, K.; Vaughan, J. Upgrading copper sulphide concentrates through high temperature metathesis reactions. In *COM 2019, Proceedings of the 58th Annual Conference of Metallurgists Hosting the 10th International Copper Conference 2019, Vancouver, BC, Canada, 18–21 August, 2019*; MetSoc: Montreal, QC, Canada, 2019; 10p.
19. Sohn, H.J.; Wadsworth, M.E. Rate processes in the secondary mineralization of copper sulfides. *Appl. Mineral.* **1984**, 485–506.
20. Bartlett, R.W.; Wilson, D.B.; Savage, B.J.; Wesely, R.J. A process for enriching chalcopyrite concentrates. In *Hydrometallurgical Reactor Design and Kinetics*; Bautista, R.G., Ed.; TMS: Warrendale, PA, USA, 1986; pp. 227–246.
21. Jang, J.H.; Wadsworth, M.E. Kinetics of hydrothermal enrichment of chalcopyrite. *ACS Symp. Ser.* **1993**, *550*, 45–58.
22. Peterson, R.D.; Wadsworth, M.E. Solid, solution reactions in the hydrothermal enrichment of chalcopyrite at elevated temperatures. In *EPD Congress*; Warren, G., Ed.; TMS: Warrendale, PA, USA, 1994; pp. 275–291.
23. Sequeira, C.A.C.; Santos, D.M.F.; Chen, Y.; Anastassakis, G. Chemical metathesis of chalcopyrite in acidic solutions. *Hydrometallurgy* **2008**, *92*, 135–140. [[CrossRef](#)]
24. Kritskii, A.; Naboichenko, S.; Karimov, K.; Agarwal, V.; Lundström, M. Hydrothermal pretreatment of chalcopyrite concentrate with copper sulfate solution. *Hydrometallurgy* **2020**, *195*, 105359.
25. Fomenko, I.V.; Pleshkov, M.A.; Shneerson, Y.M.; Ospanov, E.A.; Shakhalov, A.A.; Naboychenko, S.S. Low-grade copper concentrate purification and enrichment by complex pressure oxidation—Hydrothermal alteration technology. In *COM 2019, Proceedings of the 58th Annual Conference of Metallurgists Hosting the 10th International Copper Conference 2019, Vancouver, BC, Canada, 18–21 August, 2019*; MetSoc: Montreal, QC, Canada, 2019; 13p.
26. Viñals, J.; Fuentes, G.; Hernández, M.C.; Herreros, O. Transformation of sphalerite particles into copper sulfide particles by hydrothermal treatment with Cu (II) ions. *Hydrometallurgy* **2004**, *75*, 177–187. [[CrossRef](#)]
27. Dunn, G.M. Single Stage Pressure Leach Hydrometallurgical Method for Upgrade of Copper Concentrates. U.S. Patent Application 16/032,726, 17 January 2019.
28. Van Wyk, A.P.; Akdogan, G.; Bradshaw, S.M. Behaviour of Cu, Fe, Ni, and PGMs during leaching of Ni-Fe-Cu-S converter matte. *J. South. Afr. Inst. Min. Metall.* **2021**, *121*, 599–606. [[CrossRef](#)]
29. Dreisinger, D.B. Polymet Mining Corp. Metathetic copper concentrate enrichment. U.S. Patent 8,741,238 B2, 3 June 2014.
30. Collins, M.J.; Berezowsky, R.M.G.S.; Vardill, W.D.; Ketcham, V.J.; Stojsic, A. The Lihir Gold project: Pressure oxidation process development. In *Hydrometallurgy Fundamentals, Technology and Innovations*; Hiskey, J.B., Warren, G.W., Eds.; TMS: Littleton, CO, USA, 1993; Chapter 38; pp. 611–628.
31. Wardell-Johnson, M.; Steiper, G.; Dreisinger, D. Engineering aspects of the Platsol™ process. In *ALTA 2009 Nickel/Cobalt 14 Conference*; ALTA Metallurgical Services: Melbourne, Australia, 2009; 20p.
32. Dreisinger, D.; Murray, W.; Hunter, D.; Baxter, K.; Ferron, J.; Fleming, C. The application of the Platsol™ Process to copper-nickel-cobalt-PGE/PGM concentrates from Polymet Mining’s NorthMet Deposit. In *ALTA 2005 Nickel/Cobalt 10 Conference*; ALTA Metallurgical Services: Melbourne, Australia, 2005; 16p.
33. King, J.A.; Dreisinger, D.B.; Knight, D.A. The total pressure oxidation of copper concentrates. In *The Paul E. Queneau International Symposium Extractive Metallurgy of Copper, Nickel and Cobalt, Volume I: Fundamental Aspects*; Reddy, R.G., Weizenbach, R.N., Eds.; TMS: Warrendale, PA, USA, 1993; pp. 735–756.
34. King, J.; Dreisinger, D.B. Autoclaving of copper concentrates. In *Proceedings of Copper 95-Cobre 95, Volume III, Electrefining and Hydrometallurgy of Copper*; Cooper, W.C., Dreisinger, D.B., Dutrizac, J.E., Hein, H., Ugarte, G., Eds.; The Metallurgical Society of CIM: Montreal, QC, Canada, 1995; pp. 511–533.
35. Defreyne, J.; Grieve, W.; Jones, D.L.; Mayhew, K. The role of iron in the CESL process. In *Iron Control Technologies: Proceedings of 3rd International Symposium on Iron Control and Hydrometallurgy*; Dutrizac, J.E., Ed.; CIM: Montreal, QC, Canada, 2006; pp. 205–220.
36. Krebs, D.; Hyvarinen, O.; Dreisinger, D. Processing nickel sulphide ore or concentrates with sodium chloride. CA Patent 2624609C, 31 March 2015.
37. Lundström, M.; Liipo, J.; Aromaa, J. Dissolution of copper and iron from sulfide concentrates in cupric chloride solution. *Int. J. Miner. Process.* **2012**, *102*, 13–18. [[CrossRef](#)]
38. Abdul, B.; Asselin, E. Novel reagents for iron and sulphur control in medium temperature leaching of sulphide concentrates. *Can. Metall. Q.* **2017**, *56*, 382–392. [[CrossRef](#)]

39. Yazici, E.; Deveci, H.; Ehsani, A. Recovery of metals from chloride leach solutions of waste of printed circuit boards by adsorption and precipitation. In *Proceedings of the XXVII. International Mineral Processing Congress (IMPC 2014)*; Gecamin/International Mineral Processing Council: Santiago, Chile, 2014; pp. 170–179.
40. Zhang, R.; Mao, Y.; Liu, C.; Ni, W. Synergistic catalytic effect of chloride ion and ammonium ion on the leaching of chalcopyrite in sulfuric acid solution. *Miner. Eng.* **2022**, *185*, 107686. [[CrossRef](#)]
41. FIZ Karlsruhe—Leibniz Institute for Information Infrastructure. Inorganic Crystal Structure Database (ICSD). 2011. Available online: <http://icsd.fiz-karlsruhe.de/icsd/> (accessed on 6 March 2020).
42. International Centre for Diffraction Data. PDF-4+ 2022 Powder Diffraction File Database. Available online: <https://www.icdd.com/> (accessed on 3 May 2022).
43. Ventruti, G.; Scordari, F.; Schingaro, E.; Gualtieri, A.F.; Meneghini, C. The order-disorder character of FeOHSO<sub>4</sub> obtained from the thermal decomposition of metahohmannite, Fe<sup>3+</sup><sub>2</sub>(H<sub>2</sub>O)<sub>4</sub>[O(SO<sub>4</sub>)<sub>2</sub>]. *Am. Mineral.* **2005**, *90*, 679–686. [[CrossRef](#)]
44. Zies, E.G.; Allen, E.T.; Merwin, H.E. Some reactions involved in secondary copper sulphide enrichment. *Econ. Geol.* **1916**, *11*, 407–503. [[CrossRef](#)]
45. Young, S.W.; Moore, N.P. Laboratory studies on secondary sulphide ore enrichment, I. The copper sulphides and hydrogen sulphide. *Econ. Geol.* **1916**, *11*, 349–365. [[CrossRef](#)]
46. Young, S.W.; Moore, N.P. Laboratory studies on secondary sulphide ore enrichment, II. The formation of chalcopyrite by artificial replacement. *Econ. Geol.* **1916**, *11*, 574–581. [[CrossRef](#)]
47. Viramontes Gamboa, G.; Velásquez Roque, S.; Ibarra Bracamontes, L.A.; Gonzalez Bernal, R. Lixiviación de calcopirita en minutos. In *XXI Congreso Internacional de Metalurgia Extractiva*; Lapidus Lavine, G.T., Alonso Gómez, A.R., Fuentes Aceituno, J.C., Hernández Cruz, L., Herrera Urbina, R., Lara Castro, R.H., Luna Sánchez, R.M., Pérez Tello, M., Zárate Gutiérrez, R., Eds.; Universidad Autónoma Metropolitana: Mexico City, Mexico, 2012; pp. 336–350.
48. Byrne, K.; Hawker, W.; Vaughan, J. Department of radionuclides during copper concentrate metathesis reactions. In *ALTA 2018 23rd Annual Conference Proceedings, Uranium-REE-Lithium Conference*; ALTA Metallurgical Services: Melbourne, Australia, 2018; 12p.
49. Chaudhari, A.; Webster, N.A.; Xia, F.; Friedrich, A.; Ram, R.; Etschmann, B.; Liu, W.; Wykes, J.; Brand, H.E.; Brugger, J. Anatomy of a complex mineral replacement reaction: Role of aqueous redox, mineral nucleation, and ion transport properties revealed by an in-situ study of the replacement of chalcopyrite by copper sulfides. *Chem. Geol.* **2021**, *581*, 120390. [[CrossRef](#)]
50. Chaudhari, A.; Brugger, J.; Ram, R.; Chowdhury, P.; Etschmann, B.; Guagliardo, P.; Xia, F.; Pring, A.; Gervinskis, G.; Liu, A.; et al. Synchronous solid-state diffusion, dissolution-reprecipitation, and recrystallization leading to isotopic resetting: Insights from chalcopyrite replacement by copper sulfides. *Geochim. Cosmochim. Acta* **2022**, *331*, 48–68. [[CrossRef](#)]
51. Harmer, S.L.; Pratt, A.R.; Nesbitt, W.H.; Fleet, M.E. Sulfur species at chalcopyrite (CuFeS<sub>2</sub>) fracture surfaces. *Am. Mineral.* **2004**, *89*, 1026–1032. [[CrossRef](#)]
52. Senanayake, G. A review of chloride assisted copper sulphide leaching by oxygenated sulphuric acid and mechanistic considerations. *Hydrometallurgy* **2009**, *98*, 21–32. [[CrossRef](#)]
53. Cheng, T.C.M. Production of Hematite in Acidic Zinc Sulphate Media. Ph.D. Thesis, McGill University, Montreal, QC, Canada, 2002; 299p.
54. Reid, M.; Papangelakis, V.G. New data on hematite solubility in sulphuric acid solution from 130 to 270 °C. In *Iron Control Technologies*; Durizac, J.E., Riveros, P.A., Eds.; MetSoc: Montreal, QC, Canada, 2006; pp. 673–686.
55. Liu, H.; Papangelakis, V.G.; Alam, M.S.; Singh, G. Solubility of hematite in H<sub>2</sub>SO<sub>4</sub> solutions at 230–270 °C. *Can. Metall. Q.* **2003**, *42*, 199–208. [[CrossRef](#)]
56. Kobylin, P.M.; Sippola, H.; Taskinen, P.A. Thermodynamic modelling of aqueous Fe(II) sulphate solutions. *CALPHAD Comput. Coupling Phase Diagr. Thermochem.* **2011**, *35*, 499–511. [[CrossRef](#)]
57. Hasegawa, F.; Tozawa, K.; Nishimura, T. Solubility of ferrous sulphate in aqueous solutions at high temperatures. *Shigen Sozai* **1996**, *112*, 879–884. [[CrossRef](#)]
58. Cai, Y.; Chen, X.; Ding, J.; Zhou, D. Leaching mechanism for chalcopyrite in hydrochloric acid. *Hydrometallurgy* **2012**, *113–114*, 109–118. [[CrossRef](#)]
59. Xia, F.; Brugger, J.; Chen, G.; Ngothai, Y.; O’Neill, B.; Putnis, A.; Pring, A. Mechanism and kinetics of pseudomorphic mineral replacement reactions: A case study of the replacement of pentlandite by violarite. *Geochim. Cosmochim. Acta* **2009**, *73*, 1945–1969. [[CrossRef](#)]
60. Harmer, S.L.; Thomas, J.E.; Fornasiero, D.; Gerson, A.R. The evolution of surface layers formed during chalcopyrite leaching. *Geochim. Cosmochim. Acta* **2006**, *70*, 4392–4402. [[CrossRef](#)]
61. Senanayake, G. Chloride assisted leaching of chalcocite by oxygenated sulphuric acid via Cu(II)-OH-Cl. *Miner. Eng.* **2007**, *20*, 1075–1088. [[CrossRef](#)]
62. Pearce, C.I.; Patrick, R.A.D.; Vaughan, D.J.; Henderson, C.M.B.; van der Laan, G. Copper oxidation state in chalcopyrite: Mixed Cu d<sup>9</sup> and d<sup>10</sup> characteristics. *Geochim. Cosmochim. Acta* **2006**, *70*, 4635–4642. [[CrossRef](#)]
63. Li, Y.; Liu, Y.; Chen, J.; Zhao, C.; Cui, W. Comparison study of crystal and electronic structures for chalcopyrite (CuFeS<sub>2</sub>) and pyrite (FeS<sub>2</sub>). *Physicochem. Probl. Miner. Process.* **2021**, *57*, 100–111. [[CrossRef](#)]
64. Conejeros, S.; Alemany, P.; Lluell, M.; Moreira, I.D.P.; Sánchez, V.; Llanos, J. Electronic structure and magnetic properties of CuFeS<sub>2</sub>. *Inorg. Chem.* **2015**, *54*, 4840–4849. [[CrossRef](#)] [[PubMed](#)]

65. McDonald, G.W.; Udovic, T.J.; Dumesic, J.A.; Langer, S.H. Equilibria associated with cupric chloride leaching of chalcopyrite concentrate. *Hydrometallurgy* **1984**, *13*, 125–135. [[CrossRef](#)]
66. Lundström, M.; Liipo, J.; Taskinen, P.; Aromaa, J. Copper precipitation during leaching of various copper sulfide concentrates with cupric chloride in acidic solutions. *Hydrometallurgy* **2016**, *166*, 136–142. [[CrossRef](#)]
67. Fjellvåg, H.; Grønvold, F.; Stølen, S. Low-temperature distortion in CuS. *Z. Krist.* **1988**, *184*, 111–121. [[CrossRef](#)]
68. Conejeros, S.; Moreira, I.D.P.; Alemany, P.; Canadell, E. Nature of holes, oxidation states, and hypervalency in covellite (CuS). *Inorg. Chem.* **2014**, *53*, 12402–12406. [[CrossRef](#)] [[PubMed](#)]
69. Kalanur, S.S.; Seo, H. Synthesis of Cu<sub>x</sub>S thin films with tunable localized surface plasmon resonances. *Chem. Sel.* **2018**, *3*, 5920–5926.
70. Evans, H.T.; Konnert, J.A. Crystal structure refinement of covellite. *Am. Mineral.* **1976**, *61*, 996–1000.
71. Banerjee, N.; Krupanidhi, S.B. Facile hydrothermal synthesis and observation of bubbled growth mechanism in nano-ribbons aggregated microspherical covellite blue-phosphor. *Dalton Trans.* **2010**, *39*, 9789–9793. [[CrossRef](#)]
72. Krishnamoorthy, K.; Veerasubramani, G.K.; Rao, A.N.; Kim, S.J. One-pot hydrothermal synthesis, characterization and electrochemical properties of CuS nanoparticles towards supercapacitor applications. *Mater. Res. Express* **2014**, *1*, 035006. [[CrossRef](#)]
73. Auyoong, Y.L.; Yap, P.L.; Huang, X.; Abd Hamid, S.B. Optimization of reaction parameters in hydrothermal synthesis: A strategy towards the formation of CuS hexagonal plates. *Chem. Cent. J.* **2013**, *7*, 67. [[CrossRef](#)]
74. Patel, T.A.; Balasubramanian, C.; Panda, E. Role of reducing agent and self-sacrificed copper-thiourea complex in the synthesis of precisely controlled Cu<sub>2-x</sub>S microtubes. *J. Cryst. Growth* **2019**, *505*, 26–32. [[CrossRef](#)]
75. Mikhlin, Y.; Nasluzov, V.; Ivaneeva, A.; Vorobyev, S.; Likhatski, M.; Romanchenko, A.; Krylov, A.; Zharkov, S.; Meira, D.M. Formation, evolution and characteristics of copper sulfide nanoparticles in the reactions of aqueous cupric and sulfide ions. *Mater. Chem. Phys.* **2020**, *255*, 123600. [[CrossRef](#)]
76. Pejjai, B.; Reddivari, M.; Kotte, T.R.R. Phase controllable synthesis of CuS nanoparticles by chemical co-precipitation method: Effect of copper precursors on the properties of CuS. *Mater. Chem. Phys.* **2020**, *239*, 122030. [[CrossRef](#)]
77. Almeida, T.; Garcia, E.M.; da Silva, H.W.A.; Matencio, T.; Lins, V.D.F.C. Electrochemical study of chalcopyrite dissolution in sulfuric, nitric and hydrochloric acid solutions. *Int. J. Miner. Process.* **2016**, *149*, 25–33. [[CrossRef](#)]
78. Ghahremaninezhad, A.; Radzinski, R.; Gheorghiu, T.; Dixon, D.G.; Asselin, E. A model for silver ion catalysis of chalcopyrite (CuFeS<sub>2</sub>) dissolution. *Hydrometallurgy* **2015**, *155*, 95–104. [[CrossRef](#)]
79. Recalde Chiluiza, E.L.; Navarro Donoso, P. Chalcopyrite leaching in acidic chloride solution without sulphates. *J. Mex. Chem. Soc.* **2016**, *60*, 238–246. [[CrossRef](#)]
80. Prater, J.D.; Queneau, P.B.; Hudson, T.J. The sulfation of copper-iron sulfides with concentrated sulfuric acid. *JOM* **1970**, *22*, 23–27. [[CrossRef](#)]
81. Yang, Y.; Liu, W.; Chen, M. XANES and XRD study of the effect of ferrous and ferric ions on chalcopyrite bioleaching at 30 °C and 48 °C. *Miner. Eng.* **2015**, *70*, 99–108. [[CrossRef](#)]
82. Yang, C.; Qin, W.; Zhao, H.; Wang, J.; Wang, X. Mixed potential plays a key role in leaching of chalcopyrite: Experimental and theoretical analysis. *Ind. Eng. Chem. Res.* **2018**, *57*, 1733–1744. [[CrossRef](#)]
83. Yoo, K.; Kim, S.; Lee, J.; Ito, M.; Tsunekawa, M.; Hiroyoshi, M. Effect of chloride ions on the leaching rate of chalcopyrite. *Miner. Eng.* **2010**, *23*, 471–477. [[CrossRef](#)]
84. Gao, X.; Yang, Y.; Pownceby, M.I.; Zhong, S.; Chen, M. A sulfur K-edge XANES and Raman study on the effect of chloride ion on bacterial and chemical leaching of chalcopyrite at 25 °C. *Min. Metall. Explor.* **2019**, *36*, 343–352. [[CrossRef](#)]
85. Majuste, D.; Ciminelli, V.S.T.; Eng, P.J.; Osseo-Asare, K. Applications of in situ synchrotron XRD in hydrometallurgy: Literature review and investigation of chalcopyrite dissolution. *Hydrometallurgy* **2013**, *131*, 54–66. [[CrossRef](#)]
86. Velásquez-Yévenes, L.; Nicol, M.; Miki, H. The dissolution of chalcopyrite in chloride solutions. Part 1. The effect of solution potential. *Hydrometallurgy* **2010**, *103*, 113–118. [[CrossRef](#)]
87. Peters, E.; Loewen, F. Pressure leaching of copper minerals in perchloric acid solutions. *Metall. Trans.* **1973**, *4*, 5–14. [[CrossRef](#)]
88. Corriou, J.-P.; Kikindai, T. The aqueous oxidation of elemental sulfur and different chemical properties of the allotropic forms S<sub>λ</sub> and S<sub>μ</sub>. *J. Inorg. Nucl. Chem.* **1981**, *43*, 9–15. [[CrossRef](#)]
89. Whittington, B.I.; Muir, D.M. Pressure acid leaching of nickel laterites. A review. *Miner. Process. Extr. Metall. Rev.* **2000**, *21*, 527–599. [[CrossRef](#)]
90. Tozawa, K.; Sasaki, K. Effect of co-existing sulphates on precipitation of ferric oxide from ferric sulphate solutions at elevated temperatures. In *Iron Control in Hydrometallurgy*; Dutrizac, J.E., Monhemius, A.J., Eds.; Ellis Horwood: Chichester, UK, 1986; pp. 454–476.
91. Umetsu, V.; Tozawa, K.; Sasaki, K.-I. The hydrolysis of ferric sulphate solutions at elevated temperatures. *Can. Metall. Q.* **1977**, *16*, 111–117. [[CrossRef](#)]
92. Cheng, T.C.; Demopoulos, G.P. Hydrolysis of ferric sulfate in the presence of zinc sulfate at 200 °C: Precipitation kinetics and product characterization. *Ind. Chem. Eng. Res.* **2004**, *43*, 6299–6308. [[CrossRef](#)]
93. Habashi, F.; Bauer, E.L. Aqueous oxidation of elemental sulfur. *Ind. Eng. Chem. Fundam.* **1966**, *5*, 469–471. [[CrossRef](#)]
94. Majuste, D.; Ciminelli, V.S.T.; Osseo-Asare, K.; Dantas, M.S.S.; Magalhães-Paniago, R. Electrochemical dissolution of chalcopyrite: Detection of bornite by synchrotron small angle X-ray diffraction and its correlation with the hindered dissolution process. *Hydrometallurgy* **2012**, *111*, 114–123. [[CrossRef](#)]

95. Ruiz, M.C.; Zapata, J.; Padilla, R. Effect of variables on the quality of hematite precipitated from sulfate solutions. *Hydrometallurgy* **2007**, *89*, 32–39. [[CrossRef](#)]
96. Antonijević, M.; Bogdanović, G.D. Investigation of the leaching of chalcopyritic ore in acidic solutions. *Hydrometallurgy* **2004**, *73*, 245–256. [[CrossRef](#)]
97. Córdoba, E.M.; Muñoz, J.A.; Blázquez, M.L.; González, F.; Ballester, A. Leaching of chalcopyrite with ferric ion. Part I: General aspects. *Hydrometallurgy* **2008**, *93*, 81–87. [[CrossRef](#)]
98. Fleming, C. Basic iron sulfate. A potential killer in the processing of refractory gold concentrates by pressure oxidation. *Miner. Metall. Process.* **2010**, *27*, 81–88. [[CrossRef](#)]
99. Welham, N.J.; Malatt, K.A.; Vukcevic, S. The stability of iron phases presently used for disposal from metallurgical systems—A review. *Miner. Eng.* **2000**, *13*, 911–931. [[CrossRef](#)]
100. Nazari, G.; Dixon, D.G.; Dreisinger, D. Enhancing the kinetic of chalcopyrite leaching in the Galvanox™ process. *Hydrometallurgy* **2011**, *105*, 251–258. [[CrossRef](#)]
101. Nazari, G.; Dixon, D.G.; Dreisinger, D.B. The mechanism of chalcopyrite leaching in the presence of silver-enhanced pyrite in the Galvanox™ process. *Hydrometallurgy* **2012**, *113*, 122–130. [[CrossRef](#)]
102. Chehreghani, S.; Yari, M.; Zeynali, A.; Akhgar, B.N.; Gharegheshlagh, H.H.; Pishravian, M. Optimization of chalcopyrite galvanic leaching in the presence of pyrite and silver as catalysts by using Response Surface Methodology (RSM). *Rud.-Geološko-Naft. Zb.* **2021**, *36*, 37–47. [[CrossRef](#)]
103. Nicol, M.J. Does galvanic coupling with pyrite increase the rate of dissolution of chalcopyrite under ambient conditions? An electrochemical study. *Hydrometallurgy* **2022**, *208*, 105824. [[CrossRef](#)]
104. Javed, T.; Asselin, E. Fe (III) Precipitation and Copper Loss from Sulphate-Chloride Solutions at 150 °C: A Statistical Approach. *Metals* **2020**, *10*, 669. [[CrossRef](#)]
105. Wolska, E. The structure of hydrohematite. *Z. Krist.* **1981**, *154*, 69–75.
106. Wolska, E.; Schwertmann, U. Selective X-ray line broadening in the goethite-derived hematite phase. *Phys. Status Solidi A* **1989**, *114*, K11–K16. [[CrossRef](#)]
107. Stanjek, H.; Schwertmann, U. The influence of aluminum on iron oxides. Part XVI: Hydroxyl and aluminum substitution in synthetic hematites. *Clays Clay Miner.* **1992**, *40*, 347–354. [[CrossRef](#)]
108. Whittington, B.I.; Johnson, J.A.; Quan, L.P.; McDonald, R.G.; Muir, D.M. Pressure acid leaching of arid-region nickel laterite ore: Part II. Effect of ore type. *Hydrometallurgy* **2003**, *70*, 47–62. [[CrossRef](#)]
109. Whittington, B.I. Characterization of scales obtained during continuous nickel laterite pilot-plant leaching. *Metall. Mater. Trans. B* **2000**, *31*, 1175–1186. [[CrossRef](#)]
110. Barr, G.; Defreyne, J.; Jones, D.; Moore, R. The CESL process: Successful refining of a low grade copper concentrate. In *ALTA 2000 Copper 6 Forum, Perth*; ALTA Metallurgical Services: Melbourne, Australia, 2000; 10p.
111. Cheng, C.Y.; Lawson, F. The kinetics of leaching covellite in acidic oxygenated sulphate-chloride solutions. *Hydrometallurgy* **1991**, *27*, 269–284. [[CrossRef](#)]
112. Pollard, A.M.; Thomas, R.G.; Williams, P.A. The stabilities of antlerite and  $\text{Cu}_3\text{SO}_4(\text{OH})_4 \cdot 2\text{H}_2\text{O}$ : Their formation and relationships to other copper (II) sulfate minerals. *Mineral. Mag.* **1992**, *56*, 359–365. [[CrossRef](#)]
113. Yoder, C.H.; Agee, T.M.; Ginion, K.E.; Hofmann, A.E.; Ewanichak, J.E.; Schaeffer, C.D., Jr.; Carroll, M.J.; Schaeffer, R.W.; McCaffrey, P.F. The relative stabilities of the copper hydroxyl sulphates. *Mineral. Mag.* **2007**, *71*, 571–577. [[CrossRef](#)]
114. Zittlau, A.H.; Shi, Q.; Boerio-Goates, J.; Woodfield, B.F.; Majzlan, J. Thermodynamics of the basic copper sulfates antlerite, posnjakite, and brochantite. *Chem. Erde-Geochem.* **2013**, *73*, 39–50. [[CrossRef](#)]
115. Woods, T.L.; Garrels, R.M. Phase relations of some cupric hydroxy minerals. *Econ. Geol.* **1986**, *81*, 1989–2007. [[CrossRef](#)]
116. Pollard, A.M.; Thomas, R.G.; Williams, P.A. Connellite: Stability relationships with other secondary copper minerals. *Mineral. Mag.* **1990**, *54*, 425–430. [[CrossRef](#)]
117. Scott, D.A. A review of copper chlorides and related salts in bronze corrosion and as painting pigments. *Stud. Conserv.* **2000**, *45*, 39–53.
118. Yin, Q.; Vaughan, D.J.; England, K.E.R.; Kelsall, G.H.; Brandon, N.P. Surface oxidation of chalcopyrite ( $\text{CuFeS}_2$ ) in alkaline solutions. *J. Electrochem. Soc.* **2000**, *147*, 2945–2951. [[CrossRef](#)]
119. Azizkarimi, M.; Tabaian, S.H.; Rezai, B. Electrochemical investigation of chalcopyrite oxidation in alkaline solutions. *Sep. Sci. Technol.* **2014**, *49*, 2595–2601. [[CrossRef](#)]
120. Nicol, M.J. The electrochemistry of chalcopyrite in alkaline solutions. *Hydrometallurgy* **2019**, *187*, 134–140. [[CrossRef](#)]
121. O'Connor, G.M.; Lepkova, K.; Eksteen, J.J.; Oraby, E.A. Electrochemical behaviour and surface analysis of chalcopyrite in alkaline glycine solutions. *Hydrometallurgy* **2018**, *182*, 32–43. [[CrossRef](#)]
122. Liu, X.D.; Meng, D.D.; Zheng, X.G.; Hagihala, M.; Guo, Q.X. Mid-IR and Raman spectral properties of clinoatacamite-structure basic copper chlorides. *Adv. Mater. Res.* **2011**, *146*, 1202–1205. [[CrossRef](#)]
123. Zhao, Y.; Cui, H.; Zhang, J.; Ma, Y.; Tian, H.; Wu, L.; Cui, Q.; Ma, Y. Pressure-induced phase transformation of botallackite  $\alpha\text{-Cu}_2(\text{OH})_3\text{Cl}$  with a two-dimensional layered structure synthesized via a hydrothermal strategy. *J. Phys. Chem. C* **2020**, *124*, 9581–9590. [[CrossRef](#)]
124. Krivovichev, S.V.; Hawthorne, F.C.; Williams, P.A. Structural complexity and crystallization: The Ostwald sequence of phases in the  $\text{Cu}_2(\text{OH})_3\text{Cl}$  system (botallackite–atacamite–clinoatacamite). *Struct. Chem.* **2017**, *28*, 153–159. [[CrossRef](#)]

125. Pollard, A.M.; Thomas, R.G.; Williams, P.A. Synthesis and stabilities of the basic copper (II) chlorides atacamite, paratacamite and botallackite. *Mineral. Mag.* **1989**, *53*, 557–563. [CrossRef]
126. Sharkey, J.B.; Lewin, S.Z. Conditions governing the formation of atacamite and paratacamite. *Am. Mineral. J. Earth Planet. Mater.* **1971**, *56*, 179–192.
127. Kampf, A.R.; Sciberras, M.J.; Leverett, P.; Williams, P.A.; Malcherek, T.; Schlüter, J.; Welch, M.D.; Dini, M.; Donoso, A.M. Paratacamite-(Mg),  $\text{Cu}_3(\text{Mg,Cu})\text{Cl}_2(\text{OH})_6$ ; a new substituted basic copper chloride mineral from Camerones, Chile. *Mineral. Mag.* **2013**, *77*, 3113–3124. [CrossRef]
128. Sciberras, M.J.; Leverett, P.; Williams, P.A.; Hibbs, D.E.; Downes, P.J.; Welch, M.D.; Kampf, A.R. Paratacamite-(Ni),  $\text{Cu}_3(\text{Ni,Cu})\text{Cl}_2(\text{OH})_6$ , a new mineral from the Carr Boyd Rocks mine, Western Australia. *Aust. J. Mineral.* **2013**, *17*, 39–44.
129. Welch, M.D.; Sciberras, M.J.; Williams, P.A.; Leverett, P.; Schlüter, J.; Malcherek, T. A temperature-induced reversible transformation between paratacamite and herbertsmithite. *Phys. Chem. Miner.* **2014**, *41*, 33–48. [CrossRef]
130. Sciberras, M.J. Substitution in Basic Secondary Cu(II) Chloride Minerals. Ph.D. Thesis, University of Western Sydney, Penrith, Australia, 2013; 132p.
131. Grice, J.D.; Szymanski, J.T.; Jambor, J.L. The crystal structure of clinoatacamite, a new polymorph of  $\text{Cu}_2(\text{OH})_3\text{Cl}$ . *Can. Mineral.* **1996**, *34*, 73–78.
132. Oswald, H.R.; Guenter, J.R. Crystal data on paratacamite,  $\gamma\text{-Cu}_2(\text{OH})_3\text{Cl}$ . *J. Appl. Crystallogr.* **1971**, *4*, 530–531. [CrossRef]
133. Jambor, J.L.; Dutrizac, J.E.; Roberts, A.C.; Grice, J.D.; Szymanski, J.T. Clinoatacamite, a new polymorph of  $\text{Cu}_2(\text{OH})_3\text{Cl}$ , and its relationship to paratacamite and “anarakite”. *Can. Mineral.* **1996**, *34*, 61–72.
134. Zheng, X.G.; Kawae, T.; Kashitani, Y.; Li, C.S.; Tateiwa, N.; Takeda, K.; Yamada, H.; Xu, C.N.; Ren, Y. Unconventional magnetic transitions in the mineral clinoatacamite  $\text{Cu}_2\text{Cl}(\text{OH})_3$ . *Phys. Rev. B* **2005**, *71*, 052409. [CrossRef]
135. Malcherek, T.; Schlüter, J. Structures of the pseudo-trigonal polymorphs of  $\text{Cu}_2(\text{OH})_3\text{Cl}$ . *Acta Crystallogr. Sect. B Struct. Sci.* **2009**, *65*, 334–341. [CrossRef]
136. Vieillard, P. Propriétés thermochimiques des composés du cuivre. *Sci. Geol. Bull.* **1988**, *41*, 289–308. [CrossRef]
137. Moore, T.P. What’s new in the mineral world? The Mineralogical Record, Report #36, 2013. Available online: [https://cdn.mineralogicalrecord.com/wp-content/uploads/2020/10/whats\\_new/Toms-Online-report-36.pdf](https://cdn.mineralogicalrecord.com/wp-content/uploads/2020/10/whats_new/Toms-Online-report-36.pdf) (accessed on 24 August 2023).
138. Cook, R.B. Atacamite: Moonta Mine, South Australia, Australia. *Rocks Miner.* **2006**, *81*, 374–378. [CrossRef]
139. Gablina, I.F.; Semkova, T.A.; Stepanova, T.V.; Gor’kova, N.V. Diagenetic alterations of copper sulfides in modern ore-bearing sediments of the Logatchev-1 hydrothermal field (Mid-Atlantic Ridge 14 45’ N). *Lithol. Miner. Resour.* **2006**, *41*, 27–44. [CrossRef]
140. Chen, J.; Xu, Z.; Chen, Y. *Electronic Structure and Surfaces of Sulfide Minerals: Density Functional Theory and Applications*; Elsevier: Amsterdam, The Netherlands, 2020; 379p.
141. Speight, J. *Lange’s Handbook of Chemistry*, 16th ed.; McGraw-Hill: New York, NY, USA, 2005.
142. Reed, J.J. Digitizing “The NBS Tables of Chemical Thermodynamic Properties: Selected Values for Inorganic and C1 and C2 Organic Substances in SI Units”. *J. Res. Natl. Inst. Stand. Technol.* **2020**, *125*, 125007. [CrossRef]
143. Robie, R.A.; Hemingway, B.S. *Thermodynamic Properties of Minerals and Related Substances at 298.15 K and 1 Bar (105 Pascals) Pressure and at Higher Temperatures*; US Government Printing Office: Washington, DC, USA, 1995; Volume 2131.
144. Drouet, C.; Navrotsky, A. Synthesis, characterization, and thermochemistry of K-Na- $\text{H}_3\text{O}$  jarosites. *Geochim. Cosmochim. Acta* **2003**, *67*, 2063–2076. [CrossRef]
145. Stoffregen, R.E. Stability relations of jarosite and natrojarosite at 150–250 °C. *Geochim. Cosmochim. Acta* **1993**, *57*, 2417–2429. [CrossRef]
146. Gaboreau, S.; Vieillard, P. Prediction of Gibbs free energies of formation of minerals of the alunite supergroup. *Geochim. Cosmochim. Acta* **2004**, *68*, 3307–3316. [CrossRef]
147. Stoffregen, R.E.; Cygan, G.L. An experimental study of Na-K exchange between alunite and aqueous sulfate solutions. *Am. Mineral.* **1990**, *75*, 209–220.
148. Majzlan, J.; Dachs, E.; Benisek, A.; Plášil, J.; Sejkora, J. Thermodynamics, crystal chemistry and structural complexity of the  $\text{Fe}(\text{SO}_4)(\text{OH})(\text{H}_2\text{O})_x$  phases:  $\text{Fe}(\text{SO}_4)(\text{OH})$ , metahohmannite, butlerite, parabutlerite, amarantite, hohmannite, and fibroferrite. *Eur. J. Mineral.* **2018**, *30*, 259–275. [CrossRef]
149. Bissengaliyeva, M.R.; Ogorodova, L.P.; Mel’Chakova, L.V.; Vigasina, M.F. Thermochemical investigation of natural antlerite. *J. Therm. Anal. Calorim.* **2012**, *109*, 467–471. [CrossRef]
150. Yoder, C.H.; Flora, N.J. Geochemical applications of the simple salt approximation to the lattice energies of complex materials. *Am. Mineral.* **2005**, *90*, 488–496. [CrossRef]
151. Puigdomenech, I.; Taxén, C. Thermodynamic Data for Copper. Implications for the Corrosion of Copper under Repository Conditions. Swedish Nuclear Fuel and Waste Management Company Report, TR-00-13, 2000; 95p. Available online: [https://inis.iaea.org/search/search.aspx?orig\\_q=RN:32010691](https://inis.iaea.org/search/search.aspx?orig_q=RN:32010691) (accessed on 16 August 2023).
152. Wang, L.; Xue, N.; Zhang, Y.; Hu, P. Controlled hydrothermal precipitation of alunite and natroalunite in high-aluminum vanadium-bearing aqueous system. *Minerals* **2021**, *11*, 892. [CrossRef]
153. Ball, J.W.; Nordstrom, D.K. *User’s Manual for Wateq4f, with Revised Thermodynamic Data Base and Test Cases for Calculating Speciation of Major, Trace, and Redox Elements in Natural Waters*; Open-File Report 91-183; US Geological Survey: Reston, VA, USA, 1991; 59p.
154. Torres, C.M.; Ghorbani, Y.; Hernández, P.C.; Justel, F.J.; Aravena, M.I.; Herreros, O.O. Cupric and chloride ions: Leaching of chalcopyrite concentrate with low chloride concentration media. *Minerals* **2019**, *9*, 639. [CrossRef]

155. Martins, F.L.; Patto, G.B.; Leão, V.A. Chalcopyrite bioleaching in the presence of high chloride concentrations. *J. Chem. Technol. Biotechnol.* **2019**, *94*, 2333–2344. [[CrossRef](#)]
156. Peters, E. Direct leaching of sulfides: Chemistry and applications. *Metall. Trans. B Process Metall.* **1976**, *7*, 505–517. [[CrossRef](#)]

**Disclaimer/Publisher's Note:** The statements, opinions and data contained in all publications are solely those of the individual author(s) and contributor(s) and not of MDPI and/or the editor(s). MDPI and/or the editor(s) disclaim responsibility for any injury to people or property resulting from any ideas, methods, instructions or products referred to in the content.